TRIPLE-NEGATIVE BREAST CANCER CELLS RECRUIT NEUTROPHILS BY SECRETING TGF-β AND CXCR2 LIGANDS

1 Shuvasree SenGupta[1], Lauren E. Hein[2,3], Yang Xu[1], Jason Zhang[5], Jamie Konwerski[5], Ye Li[4], Craig
2 Johnson[4], Dawen Cai[4], Janet Smith[5,6], and Carole A. Parent[1,2,4,6]

3 [1] Department of Pharmacology, University of Michigan Medical School

4 [2]Cancer Biology Graduate Program, [3] Rogel Cancer Center, University of Michigan

5 [4] Department of Cell and Developmental Biology, University of Michigan Medical School

6 [5] Department of Biological Chemistry, University of Michigan Medical School

7 [6]Life Sciences Institute, University of Michigan

8 *** Correspondence:**
9 Carole Parent
10 parentc@umich.edu

11 **Keywords:** TNBC, neutrophil, chemotaxis, tumor spheroid, TGF-β, GRO, CXCR2

12 **Number of words:** ~8000

13 **Number of figures:** 8

14 **Number of supplemental figures:** 5

15 **Number of supplemental movies:** 10

16 **Number of tables:** 1

17 **Running title:** Neutrophil chemotaxis in breast cancer

Abstract

Tumor associated neutrophils (TANs) are frequently detected in triple-negative breast cancer (TNBC). Recent studies also reveal the importance of neutrophils in promoting tumor progression and metastasis during breast cancer. However, the mechanisms regulating neutrophil trafficking to breast tumors are less clear. We sought to determine whether neutrophil trafficking to breast tumors is determined directly by the malignant potential of cancer cells. We found that tumor conditioned media (TCM) harvested from highly aggressive, metastatic TNBC cells induced a polarized morphology and robust neutrophil migration, while TCM derived from poorly aggressive estrogen receptor positive (ER+) breast cancer cells had no activity. In a three-dimensional (3D) type-I collagen matrix, neutrophils migrated toward TCM from aggressive breast cancer cells with increased velocity and directionality. Moreover, in a neutrophil-tumor spheroid co-culture system, neutrophils migrated with increased directionality towards spheroids generated from TNBC cells compared to ER+ cells. Based on these findings, we next sought to characterize the active factors secreted by TNBC cell lines. We found that TCM-induced neutrophil migration is dependent on tumor-derived chemokines, and screening TCM elution fractions based on their ability to induce polarized neutrophil morphology revealed the molecular weight of the active factors to be around 12 kDa. TCM from TNBC cell lines contained copious amounts of GRO (CXCL1/2/3) chemokines and TGF-β cytokines compared to ER+ cell-derived TCM. TCM activity was inhibited by simultaneously blocking receptors specific to GRO chemokines and TGF-β, while the activity remained intact in the presence of either single receptor inhibitor. Together, our findings establish a direct link between the malignant potential of breast cancer cells and their ability to induce neutrophil migration. Our study also uncovers a novel coordinated function of TGF-β and GRO chemokines responsible for guiding neutrophil trafficking to the breast tumor.

Introduction

Neutrophils are increasingly recognized as critical tumor-infiltrating immune cells [1]. As part of the innate immune system, they rapidly navigate to sites of infection or tissue injury. Upon arrival to the infected/injured sites, the primary functions of neutrophils are to eliminate invading pathogens and mount an inflammatory response using diverse mechanisms, ranging from phagocytosis and respiratory burst, to the release of toxic granule contents and DNA-containing neutrophil extracellular traps (NET) [2]. Apart from these defense functions, neutrophils have gained attention for their newly discovered role at either promoting [3-5] or hindering [6-8] tumor progression, depending on the types of cancer. The metastasis promoting function of neutrophils during breast cancer have been attributed to the suppression of anti-cancer adaptive immunity [9], stimulation of tumor cell growth [3, 10, 11], or tumor cell invasion and migration ability [4, 12-14]. Tumor-associated neutrophils (TANs) have been detected in varying degrees in the tumor niche of various kinds of malignancies [15], including breast cancer [16, 17]. Yet, cancer-associated guidance cues that drive neutrophil migration to the breast tumor niche are not well defined, partly because of the molecular heterogeneity among different breast cancer subtypes [18].

The major molecular subtypes of breast cancer are luminal A, luminal B, HER2 positive, and triple-negative breast cancer (TNBC), which widely differ in the expression of estrogen hormone receptor (ER), progesterone hormone receptor (PR), and overexpression of human epidermal growth factor receptor-2 (Her-2/neu) [18]. The predominant luminal subtypes are characterized by the presence of hormone receptors (HR+), and exhibit a relatively less aggressive clinical outcome [19]. In contrast, TNBC tumors, which comprise ~15-20% of all breast cancers, are notoriously aggressive with poor clinical outcome, and the occurrence of early distal metastasis is common [20]. Because of the lack of the receptors commonly targeted by existing targeted therapies, the primary therapeutic options for TNBC patients are currently restricted to chemotherapy. However, recent encouraging outcomes with a subset of TNBC subtypes [21] using immune-based strategies have prompted focus on characterizing the immune landscape of the breast tumor niche more comprehensively. Importantly, accumulating evidence has recently highlighted the importance of myeloid cells in regulating the responses of lymphoid populations [22, 23]. Moreover, recent studies have reported the frequent presence of TANs in the tumor niche of TNBC subtypes [16, 17]. In contrast, relatively less aggressive, hormone receptor-positive (HR+) breast tumors have fewer TANs [16], pointing toward an association between the malignant potential of breast cancer cells and the degree of neutrophil recruitment to tumors.

Neutrophils are specially equipped with the ability to directionally migrate toward chemical guidance cues, a process referred to as chemotaxis. They undergo chemotaxis by sensing gradients of chemical cues that bind and activate their cognate receptors, which induce polarized morphology and directed migration [24]. Both tumor and stromal cells are capable of secreting chemokines, cytokines, and growth factors, which in turn facilitate neutrophil mobilization to the tumor niche [25-27]. However, it remains unknown whether tumor cell intrinsic differences in the expression pattern of guidance cues are the sole determinant of the differential presence of TANs in different molecular subtypes of breast cancers.

In the present study, we compared the neutrophil recruitment abilities of tumor-conditioned media (TCM) derived from breast cancer cell lines representing either TNBCs or estrogen receptor positive (ER+) subtypes that constitute the majority of HR+ breast cancer [28, 29]. We followed neutrophil migration in real time in 3 dimensional (3D) collagen matrices towards TCM and determined how tumor-secreted factors modulate neutrophil velocity and directionality. In addition, by establishing a neutrophil-tumor spheroid co-culture system, we observed the ability of breast cancer cells to directly

87 recruit neutrophils. Most importantly, we characterized the nature of the active factors secreted from
88 breast cancer cells using a number of pharmacological, biochemical, and immunological approaches,
89 and identified the factors responsible for neutrophil recruitment by breast tumor.

90 Materials and Methods

91 *Materials*

92 Formyl-methionyl-leucyl-phenylalanine or fMLF (F3506), DMSO, and Pertussis toxin (PT, P7208)
93 were purchased from Sigma-Aldrich. Human recombinant CXCL8 (CHM349), CXCL1 or GROα
94 (CHM329) and GM-CSF (CYT-838) were purchased from ProSpec.

95 *Cell cultures*

96 We used a panel of 13 different cell lines of breast epithelial origin in the study. Cell lines of different
97 receptor expression status and malignant potential were cultured using medium and serum described
98 in Table 1. All cell lines were maintained at 37°C with 5% CO_2 except SUM149 cells, which were
99 maintained with 10% CO_2 [30]. All cell lines tested negative for mycoplasma contamination using
100 the Mycoalert detection kit (Lonza).

101 *Isolation of human neutrophils*

102 Blood was obtained from healthy human male and female subjects aged 19–65 years, through the
103 Platelet Pharmacology and Physiology Core at the University of Michigan. The Core maintains a
104 blanket IRB for basic science studies, where HIPAA information is not required. Therefore, while the
105 IRB-approved Core enrolls healthy subjects that conform to the protection of human subject
106 standards, we did not have access to this information. The samples that we received were fully de-
107 identified. Neutrophils were purified using dextran-based sedimentation followed by histopaque-
108 based density gradient centrifugation, adapted from the method described previously [31, 32].
109 Endotoxin free (< 0.005 EU/mL) cell culture grade water (SH30529, Cytiva) was used to dilute any
110 reagents used for neutrophil isolation from the blood. All tubes used were coated with 0.5% tissue
111 culture grade BSA (A9576, Sigma-Aldrich) diluted in DPBS in order to prevent non-specific cell
112 activation by adhesion to the tube wall. Isolated neutrophils were cleared off residual red blood cells
113 by ACK lysis buffer (10-548E, Lonza) and resuspended in mHBSS buffer (20mM HEPES, pH 7.4,
114 150mM NaCl, 4 mMKCl, 1.2mM MgCl2, and 10 mg/ml glucose). Viable cells were counted using
115 0.01% trypan blue (SV30084.01, Cytiva). Cells were more than 99% viable immediately following
116 isolation. In order to address donor-to-donor variability of neutrophil response, cells were routinely
117 tested for minimum basal activity and a robust response to fMLF stimulation before proceeding with
118 daily studies. A dose dependent conversion from basal circular to elongated polarized morphology of
119 fMLF stimulated neutrophils were confirmed by bright-field imaging of two randomly selected fields
120 using 40x objective lens on a Zeiss Axiovert microscope.

121 *Tumor spheroid generation*

122 Tumor spheroids were generated using the hanging drop method [33]. Briefly, 1000 cancer cells
123 resuspended in full serum media were seeded in 20 µl drops on the inside surface of petri dish lids.
124 Lids were then inverted and placed onto media filled dishes. Spheroids were grown for 4 days in the
125 incubator at 37°C. Day-4 spheroids, visible as aggregates at the bottom of each hanging drop were
126 harvested and used either for imaging or to generate TCM.

127 *Spheroid imaging*

128 Tumor spheroids were imaged using a 2-photon microscopy. Briefly, day-4 spheroids were fixed with
129 4% PFA for 1 hour at room temperature. Spheroids were stained with DRAQ5 (Abcam #108410)

130 (1:1000) overnight at 4°C and then mounted onto poly-L-lysine coated coverslips. To reduce scattered
131 light and improve image quality, the spheroids were optically cleared using the ultrafast optical
132 clearing method (FOCM) [34]. Lastly, the coverslips were mounted onto glass slides using
133 ImmuMount (Thermo Scientific #9990402) with small spacers between the slides and the coverslips
134 to prevent the spheroids from being flattened. The spheroids were imaged at 1040 nm using a C-Plan
135 Apochromat 40x/1.3x oil objective on a Zeiss LSM 780. Image stacks were first processed by
136 Histogram Matching with nTracer-AlignMaster [35] to equate brightness differences among slices
137 within the same stack. A median filter with a radius of 0.5px was then applied to suppress the
138 background noise. Center slices of each image stacks were used to representatively demonstrate the
139 spheroids' structure from each cell type. Movies traversing the image stacks from top to bottom were
140 also generated.

141 *Harvesting conditioned media from 2D culture*
142 To generate conditioned media (CM or TCM), cell lines were seeded at a density of $0.15X10^6$/ml in
143 2 ml (6-well tissue culture plate), 16 ml (T75 tissue culture flask), or 32 ml (T150 tissue culture dish)
144 volume of complete medium for 24 hrs, at which point they reached ~ 70% confluence. The culture
145 medium was then removed and cells were gently washed twice with calcium and magnesium free
146 sterile DPBS (Gibco) to remove left over serum containing media. Cells were then incubated with
147 fresh medium supplemented with reduced serum (1%) (Fig.1A) or without serum (Fig.2A) and
148 incubated for an additional 24 or 48 hrs, respectively. The media was then harvested and filtered
149 through 0.22 µm membrane filter to remove dead cell debris. Aliquots were frozen at -30°C until
150 analyzed.

151 *Harvesting conditioned media from 3D spheroid culture*
152 To generate TCM from cells grown in 3D spheroids, approximately 30 day-4 spheroids were placed
153 in each well of poly-HEMA-coated, 96-well, V-bottom plates. Once settled to the bottom, spheroids
154 were gently rinsed with DPBS and incubated in 200 µl serum-free media for 48 hrs. The media was
155 then harvested and filtered through a 0.22 µm membrane filter. Aliquots were frozen at -30°C until
156 analyzed.

157 *Neutrophil polarized morphology analysis by immunofluorescence*
158 For the analysis of actin polymerization and polarized morphology, neutrophils were seeded at 1-
159 $2x10^6$ cells/ml in 1 ml volume in a 35 mm dish with 20 mm #1.5 coverslip (MatTek). The coverslips
160 were pre-coated with 25 µg/ml fibrinogen (F4883, Sigma-Aldrich) in DPBS for 1 hr at 37°C.
161 Neutrophils were incubated 5-10 min in the incubator at 37°C to allow floating cells to settle down
162 on the coverslip. Cells were then stimulated with an equal volume of TCM, media control, positive
163 control fMLF or vehicle control DMSO and were further incubated for 15-20 min at 37°C. Following
164 stimulation, the entire liquid medium was gently discarded from each dish and the adherent cells were
165 immediately fixed with 4% PFA (Electron Microscopy Sciences), 0.1% glutaraldehyde (G5882,
166 Sigma-Aldrich), 5% sucrose (BP220, Fisher Scientific), and 0.1M cacodylate (11652, Electron
167 Microscopy Sciences), for 15 min at room temperature (RT). Once fixed, cells were washed with
168 0.1M glycine (G8898, Sigma Aldrich) in DPBS to quench the autofluorescence of glutaraldehyde.
169 Washed cells were next permeabilized with 0.05% saponin (84510, Sigma Aldrich) in 3% BSA-
170 containing DPBS for 15 min at RT and stained with phalloidin-TRITC (P1951, Sigma Aldrich) and
171 DAPI (D9542, Sigma Aldrich). Cells were imaged using a 63x objective lens on a Zeiss LSM880
172 confocal microscope. Cells in three to five different fields across the coverslip were captured
173 randomly per condition in each experiment. F-actin polymerization and cell circularity were measured
174 using the ImageJ image analysis software. Briefly, integrated density, which is a product of cell area
175 and mean fluorescence intensity, and circularity were obtained from ImageJ after manually

176 identifying the boundary of each cell in a given field. Polarization index was calculated by
177 normalizing the integrated density of each cells with respect to the positive control (fMLF) in each
178 experiment.

179 *Neutrophil polarized morphology analysis by bright-field microscopy*
180 To analyze cell circularity in response to TCM fractions or TCM in the presence of inhibitors,
181 $0.15x10^6$ neutrophils were seeded in each well of a fibrinogen coated 8 well chambered cover glass
182 with #1.5 cover glass (Cellvis). Cells were allowed to adhere to the cover glass by incubating at
183 37°C/5% CO_2 for 5 min followed by stimulation with an equal volume of TCM fractions, controls or
184 TCM with or without the inhibitor for an additional 15 min at 37°C/5% CO_2. Bright-field images of
185 the cells in two to three randomly selected fields per condition were captured using a 40x objective
186 lens on a Zeiss Colibri microscope. Circularity of each cell was measured by identifying cell boundary
187 manually using ImageJ software.

188 *Transwell assay*
189 To quantify the ability of TCM to induce neutrophil migration, transwell migration chambers with
190 membrane inserts of 3 µm diameter pore size (Corning and Greiner Bio-One) were used. Both the
191 inserts and the bottom wells were coated with 2% tissue culture grade BSA for 1 hr at 37°C to prevent
192 strong neutrophil adhesion. Coated inserts and wells were rinsed with DPBS twice to remove residual
193 BSA. Freshly isolated neutrophils at a density of $4X10^6$/ml were seeded onto the inserts (100 or 200
194 µl), and placed in 24-well or 12-well plates, respectively. Control chemoattractants or TCM were
195 gently added in 600 or 1200 µl volume to the bottom wells of 24-well or 12-well plates, respectively,
196 avoiding any bubble formation between the insert and the liquid in the well. Migration was allowed
197 to take in 37°C/5% CO_2 for 2 hrs. The percentage of neutrophils migrated to the bottom chamber was
198 calculated from the cell counts obtained using a hemocytometer.

199 *Under agarose assay*
200 Under agarose migration assay was performed following the protocol described elsewhere [36].
201 Briefly, 0.5% SeaKem ME agarose (Lonza) in 50% each of DPBS and mHBSS was poured and
202 allowed to solidify in 1% BSA-coated 35 mm glass bottom dish with 20 mm micro-well #1.5 cover
203 glass (Cellvis). Using a metallic hole punching tool, three 1 mm diameter wells were carved out at a
204 2 mm distance from each other. Neutrophils were stained with 0.5 µM CellTracker Red CMPTX dye
205 (Invitrogen) for 15 min at 37°C in rotation and re-suspended in mHBSS. In some experiments, cells
206 were pre-treated with pertussis toxin (PT) for 2 hrs followed by staining in PT supplemented buffer.
207 7 µl (5×10^4 cells) of stained cells were added to the wells at the edges and cells were allowed to
208 migrate towards the center well containing 7 µl of either fMLF (100 nM) or 50 µg/ml of GM-CSF for
209 2 hrs at 37°C/5% CO_2. End point images of cells migrating towards the chemoattractant were acquired
210 using a 10x objective lens (Zeiss Axiovert microscope).

211 *3D collagen matrix assay*
212 Migration in 3D matrix of type I collagen was performed as previously described [37]. Briefly,
213 neutrophils were fluorescently labeled by staining with 0.5 µM CellTracker Red CMTPX dye
214 (Invitrogen) for 15 min at 37°C in rotating condition. Collagen mix was prepared on ice by adding
215 sodium bicarbonate (S8761, Sigma Aldrich), MEM (10X, M3024, Sigma Aldrich), and Purecol® (3
216 mg/mL, 5005, Advanced Biomatrix) in a 1:2:15 ratio. Labeled cells were washed and resuspended in
217 1x mHBSS. $0.5x10^6$ labeled cells were gently added to the collagen mix such that the final
218 concentration of collagen is 0.2%. The collagen-cell mix was then immediately added to fill two-
219 thirds of a migration chamber made of coverslip and glass slide. The slide with the chamber was then
220 placed in upright position in the incubator at 37°C/5% CO_2 for at least 20 min to allow for the gel to

221 polymerize. The upper one-third empty space of the chamber was filled with chemoattractant, either
222 TCM or controls such as media, CXCL8 or buffer. The chamber was immediately sealed with paraffin
223 mix. Time-lapse video was captured for 40 mins at different positions (see Fig. 3A) across the
224 boundary of the chemoattractant and collagen-cell mix using an environmental controlled Zeiss LSM
225 880 at 10x magnification with the pinhole open. The Manual Tracking plugin in ImageJ software was
226 used to analyze the migration data, where about 70-100 cells were manually tracked over the 40 min
227 time course in each of three randomly selected positions per condition in each experiment. For CXCL8
228 and buffer control, cells located 1 to 1.5 mm below the matrix boundary were tracked as cells near the
229 boundary mostly exhibited random slow migration, possibly because high concentration of CXCL8
230 in the boundary saturates the receptors (CXCR1/2). In contrast, cells in the immediate vicinity of the
231 boundary (~500 µm) showed maximum directional movement for TCM and were tracked for both
232 TCM and media control. The software quantified the velocity and directionality of migration, where
233 the directionality was represented by X-FMI, which reflects the efficiency of forward migration of
234 the cells parallel to the gradient [38].

235 *Tumor spheroid-neutrophil co-culture assay*
236 To evaluate neutrophil recruitment toward cancer cells in real time, a co-culture model system was
237 developed (Fig. 5A). Wells of a 24 well glass-bottom plate (Cellvis P24-1.5H-N) were coated with
238 200 µg/ml fibronectin (Sigma-Aldrich F1141) for at least 1 hr at 37°C. Approximately 20 spheroids
239 resuspended in 250 µl fresh media (Table 1) supplemented with reduced serum (1%) were plated in
240 each well. Spheroids were allowed to attach to the plate for about 4 hrs in the incubator at 37°C/5%
241 CO_2. Towards the end of incubation, neutrophils were primed with 5 ng/ml GM-CSF for 30 mins.
242 $5x10^4$ or $1x10^5$ primed neutrophils were seeded to each well in 250 µl of 1% serum media. Multiple
243 spheroids in each well were imaged for 24 hrs using an environmental controlled Zeiss Colibri
244 microscope at 10x magnification. To analyze the migration of the neutrophils, the paths of at least 40
245 neutrophils per video, spaced out both spatially and temporally, were manually tracked using the
246 Manual Tracking plugin in ImageJ software. The position data acquired from the tracking were used
247 in a custom MATLAB script to quantify X-FMI.

248 *Treatment with pertussis toxin*
249 Neutrophils were treated with pertussis toxin as previously described [39]. Briefly, $4x10^6$
250 neutrophils/ml were pre-incubated in mHBSS with 10% heat inactivated fetal bovine serum without
251 or with 500 ng/ml pertussis toxin for 2 hours at 37°C with gentle rotation. After 2 hrs, the cells were
252 centrifuged and the pellet was resuspended in mHBSS with 0.5% BSA with or without pertussis toxin.
253 The cells were then loaded into transwell inserts and their migration was assessed as described above.

254 *TCM fractionation by size exclusion chromatography*
255 30 ml serum free TCM was collected from M4 and MDA-MB-231 cell lines as described above. TCM
256 was concentrated 100-120 fold using Amicon Ultra-15 centrifugal tubes (Millipore Sigma) of 3 kDa
257 molecular weight cut-off. Briefly, 15 ml TCM was centrifuged at 4000 rpm for 40 min at RT. Filtrates
258 were discarded and an additional 15 ml TCM was added to the resulting concentrate, mixed well and
259 centrifuged as before. The final concentrate was buffer exchanged twice with sterile DPBS to get rid
260 of the residual media components and frozen at -30°C until use. Concentrated TCM was applied to a
261 30 cm x 10 mm Superdex 75 10/300 column (GE Life Sciences) equilibrated with 30 ml DPBS. The
262 column was calibrated using four standards: aprotinin MW 6.5 kDa (Sigma-Aldrich, A3886),
263 cytochrome c MW 12.4 kDa (Sigma-Aldrich, C7150), carbonic anhydrase MW 29 kDa (Sigma-
264 Aldrich, C7025), and bovine serum albumin MW 66 kDa (Sigma-Aldrich, A8531). Sample was run
265 at a rate of 0.2 ml/min and fractions of 150 µl were collected using DPBS as an eluent. Fractions were
266 stored at 4°C until use.

267 *Multiplex ELISA array*
268 TCM concentrates were sent to RayBiotech, Inc. (GA) to screen for a panel of potential neutrophil
269 chemoattracting factors encompassing CXCL chemokine family members CXCL1/2/3 aka GRO,
270 CXCL5, CXCL6, CXCL8, CXCL12, CCL family members CCL2, CCL3, CCL5, growth factors G-
271 CSF, GM-CSF, and cytokine TGF-β. The presence of the analytes was detected and quantified using
272 a high throughput custom Quantibody multiplex enzyme-linked immunosorbent assay (ELISA)
273 (RayBiotech) and the data were analyzed by RayBiotech, Inc. Briefly, concentrates were prepared as
274 described above using 60 ml serum free TCM harvested from the respected cell lines such that the
275 protein concentration approximated 1-2 mg/ml, as estimated using the Pierce BCA protein assay kit
276 (Thermo Fisher). Concentrated samples were tested without dilution in quadruplicate, as per the
277 manufacturer instructions. The protein concentration for each target analyte was quantified by
278 comparing the fluorescence signal from the sample with the individual standard curve generated by
279 known concentrations of each protein.

280 *Western blotting analysis*
281 ERK phosphorylation was assessed using western blotting analysis. In brief, neutrophils were
282 pretreated with 2 mM pefabloc protease inhibitor (Sigma Aldrich) for 15 min at 37°C with gentle
283 rotation. $4x10^6$ neutrophils/ml were seeded in 500 µl in each well of a 12 well tissue-culture plate pre-
284 coated with 25 ug/ml fibrinogen. Cells were allowed to settle down in the well by incubating the plate
285 for 5 min at 37°C. Cells were then exposed to an equal volume of TCM, media control, positive
286 controls including fMLF and CXCL1 or the corresponding vehicle controls. After 5 min stimulation
287 at 37°C/5% CO_2, the plate was placed on ice and the cells were lysed in 1X Laemmli buffer (Biorad)
288 containing 5% β-mercaptoethanol (VWR), phoSTOP (Millipore Sigma) and Halt^{tm} protease and
289 phosphatase inhibitor cocktails (Thermo Scientific) at 95°C for 10 min. An equal volume of each was
290 resolved by 10% SDS–PAGE, transferred onto PVDF membranes (Millipore), blocked with 5%
291 nonfat dry milk for 1 hr and probed with primary Abs: phospho-p44/42 MAPK (ERK1/2)
292 (Thr202/Tyr204, dilution 1:2000, Cell Signaling Technology cat. no. 4370) and alpha tubulin (dilution
293 1:2000, Proteintech Cat no. 66031-1-Ig). Bands were visualized using HRP-conjugated secondary
294 antibodies (dilution 1:8000, Jackson ImmunoResearch), SuperSignal™ West Pico PLUS
295 Chemiluminescent Substrate, and a C600 digital imaging system (Azure). Integrated density for each
296 band was measured using ImageJ software.

297 *Neutrophil inhibition*
298 Neutrophils were pre-treated with the CXCR2 receptor antagonist AZD5069 (Cayman Chemical), the
299 TGF-β1 receptor ALK5 antagonist SB431542 (Cayman Chemical), or the SMAD3 phosphorylation
300 inhibitor SIS3 (Cayman Chemical) at 1 µM, 1 µM and 3 µM, respectively, or with vehicle control
301 DMSO for 30 min at 37°C with gentle rotation before they were added to the polarization or transwell
302 migration assay.

303 *Lactate dehydrogenase (LDH) assay*
304 Cancer cell membrane integrity was analyzed for the detection of cell death using the LDH
305 cytotoxicity assay kit (Thermo Scientific) based on the manufacturer instructions. Briefly, cancer cells
306 were seeded at $0.15x10^6$ cells/ml in 100 µl volume in a 96-well tissue culture dish in two sets of
307 triplicate wells. The control set was for maximum LDH release by subjecting cells to undergo
308 complete lysis, and the test set was for spontaneous LDH release. Cells were subjected to incubation
309 and subsequent media change as described for generating serum free TCM. Three days after initial
310 seeding, 10 µl of 10x lysis buffer and 10 µl of sterile water were added to the control and test set,
311 respectively. After incubating the plate for 45 min in the incubator at 37°C/5% CO_2, 50 µl from each

312 well was transferred to a fresh 96 well plate, mixed with 50 µl LDH reaction mix, and incubated for
313 additional 30 min at RT protected from light. Finally, the reaction was stopped by adding the stop
314 solution and absorbance was measured at 490nm and 680nm by a SpectraMax M5 Multi-Mode
315 Microplate Reader (Molecular Devices). Absorbance was corrected by subtracting background signal
316 of the instrument followed by correcting for the absorbance values of corresponding media. The
317 percentage of maximum LDH release was calculated with respect to corresponding control set.

318 *Cancer cell migration and invasion assay*
319 Endpoint migration and invasion assays were performed using a transwell system in 24-well plates
320 (Falcon, #353504). FluoroBlock™ filter inserts (Corning, #351152) with 8 µm pore size were used
321 that block light transmission from 400-700 nm and allow fluorescence detection only from the cells
322 that migrated/invaded to the bottom side of the inserts with a bottom-reading fluorescence plate
323 reader. The inserts were uncoated for the migration assays, and coated for the invasion assays with
324 0.2 mg/ml type I bovine collagen PureCol® of which the pH was neutralized to 7.2 – 7.4 using sodium
325 bicarbonate. Cancer cells that were serum starved for 24 hrs were seeded onto the inserts at $0.5x10^5$
326 cells/ml in 100 µl of serum free media. Cells were allowed to migrate toward the bottom chamber
327 containing 500 µl of full-serum media as the chemoattractant or serum-free media as the negative
328 control. After a 24 hr incubation at 37°C/5% CO_2, the inserts were transferred to a fresh 24-well plate
329 with black walls containing 500 µl of 4 µM Calcein AM (Biotium) in mHBSS per well. Cells were
330 incubated for 1 hr at 37°C, and the fluorescence reading of migrated/invaded cells was measured from
331 the bottom at wavelengths of 495/515 nm (Excitation/Emission) by a SpectraMax M5 Multi-Mode
332 Microplate Reader (Molecular Devices).

333 *Bioinformatics*
334 The transcript expression levels of different CXL chemokine family members in breast cancers were
335 analyzed using datasets identified from the cancer microarray database Oncomine
336 (http://www.oncomine.org). A total of 7 datasets from independent studies were selected from a list
337 of studies obtained by setting the search thresholds as follows: Data type, mRNA; gene rank, top 10%;
338 fold change, 2; P-value, 0.0001. Studies that used Affymetrix platforms other than hgu133plus2 and
339 hgu133a were excluded from further analysis. For each of the studies analyzed, data were downloaded
340 from GEO per instructions of the respective publications. Farmer [40], Minn [41], Wang [42], Ivshina
341 [43] used the Affymetrix hgu133A array while Miyake [44], Schuetz [45], Kao [46] used the
342 Affymetrix hgu133plus2.0 array. For the Schuetz dataset [45], we could not get the raw CEL files and
343 subsequently started from the expression matrix provided with the GEO download. CEL files for all
344 other projects were processed using the Robust Multi-array Average (RMA) technique to obtain
345 normalized expression values [47]. Estrogen receptor annotation was obtained from the data
346 download or from Ivshina [43], Wang [42], Minn [41], Miyake [44], Schuetz [45], and Farmer [40]
347 datasets. Estrogen receptor annotation was not provided for Kao [46]. Instead, using simple
348 histograms, the cutoff for ER status was set by visually selecting a point between the bimodal
349 distribution of ER expression; that cutoff was 10. The Limma package of Bioconductor was used to
350 fit linear models to each dataset comparing ER- samples to ER+ [48]. For Schuetz [45], the model
351 controlled for variation from ductal carcinoma in situ (DCIS) and invasive ductal carcinoma (IDC)
352 status. No other study had a co-variate considered. Data for CXCL chemokines were extracted and
353 the log2 fold change between ER- and ER+ were plotted in a heatmap along with the fold change for
354 the datasets respective estrogen receptor 1 (ESR1) gene (probeset 205225_at). Samples (columns)
355 were sorted by ESR1 expression. From the TCGA data portal, we used the search "Project id" IS
356 "TCGA-BRCA" AND "Workflow Type" IS "HTSEQ-FPKM" AND "Data Category" IS
357 "Transcriptome Profiling" to find 1,222 FPKM (fragments per kilobase of exon model per million

358 reads mapped) data files. The log2 of the FPKM values were plotted for our chemokines of interest
359 and samples were ordered by the FPKM of ESR1.

360 *Statistical analysis*
361 GraphPad Prism software was used for data plotting and conducting statistical analysis by tests that
362 are described in the respective figure legends along with the size of the samples. Tests used included
363 two-tailed paired t test, unpaired t test, 1-way ANOVA with Dunnett's multiple comparisons test or
364 2-way ANOVA with Sidak's multiple comparisons test.

365 **Results**
366 **Condition media derived from TNBC cell lines induce neutrophil migration**

367 Numerous studies have suggested that soluble factors, such as CXCL chemokine family members,
368 promote neutrophil infiltration in a variety of tumors. For example, CXCL members CXCL8 (aka IL-
369 8) and CXCL1/2 have been implicated in driving neutrophil recruitment in breast cancer [49-52], and
370 overexpression of these chemokines is associated with breast tumor samples and breast cancer cell
371 lines that have negative estrogen receptor expression status and higher aggressiveness [50, 53-55].
372 We confirmed these observations by comparing the expression pattern of all known CXCL
373 chemokines across breast cancer subtypes that differ in ER expression status by analyzing
374 transcriptome-based expression data identified from Oncomine and TCGA databases (Fig. S1). Out
375 of 12 CXCL chemokines, we found that the expression of CXCL8, CXCL1, and CXCL2 transcripts
376 was significantly elevated in ER- breast cancer specimens compared to ER+ samples in seven, four
377 and three independent studies, respectively (Fig. S1C). Similarly, TCGA data analysis revealed
378 elevated expression patterns of CXCL8, CXCL1, and CXCL5 in ER- breast cancer specimens (Fig.
379 S1D).

380 The differential chemokine expression pattern detected among breast cancer subtypes prompted us to
381 investigate the neutrophil recruiting ability of a panel of breast cancer cell lines that differ in ER
382 expression status and malignant potential. TNBCs and ER+ breast cancer cell lines along with non-
383 malignant M1 and metastatic derivative M4 cells from the MCF10A breast cancer progression model
384 [56-59] (Table 1) were cultured *in vitro* under identical seeding cell density. The higher malignant
385 potential of the TNBC cell lines compared to the ER+ breast cancer cell lines was confirmed by
386 assessing their migration and invasion abilities (Fig. S2A&B). We harvested TCM after growing cells
387 in serum reduced media for 24 hrs (Fig. 1A), and tested the ability of the TCM to activate neutrophils.
388 Neutrophils stimulated with fMLF, which is a formylated bacterial tripeptide and a potent neutrophil
389 chemoattractant [32], exhibited an elongated morphology with strong F-actin accumulation in the
390 protrusions, detected using fluorescently tagged phalloidin [32] (Fig. 1Bii; quantified in Fig. 1C&D).
391 In contrast, the majority of neutrophils exposed to DMSO control maintained a circular shape similar
392 to resting neutrophils, and a uniform distribution of cortical actin (Fig. 1Bi). Similar to fMLF, TCM
393 derived from metastatic M4 cells induced strong polarized morphology and F-actin depositions at the
394 poles (Fig. 1Bv; quantified in Fig. 1C&D), while most of the cells stimulated with condition media
395 (CM) collected from M1 cells remained circular (Fig. 1Biv; quantified in Fig. 1C&D). In addition,
396 we found a significant decrease in circularity and increase in F-actin intensity of neutrophils
397 stimulated with TNBC BT549 cell-derived TCM, while TCM derived from ER+ BT474 cells failed
398 to induce such changes (Fig. 1C&D). Next, we assessed the ability of the TCM to induce neutrophil
399 migration using a transwell setup (Fig. 1E). Similar to the polarization response, we found that a

400 significant proportion of neutrophils migrated toward TCM derived from metastatic M4 and TNBC
401 cells, but not from ER+ cells (Fig. 1F). Because each breast cancer cell line has a unique genetic
402 background, we also included in our panel bone-, lung- and brain-specific highly metastatic MDA-
403 MB-231 cells selected from the same parental MDA-MB-231 TGL cells [41, 60, 61]. Interestingly,
404 neutrophil migration towards TCM derived from lung- and bone-specific MDA-MB-231 cells was
405 significantly higher than towards TCM from the relatively less metastatic MDA-MB-231 TGL
406 parental line (Fig. 1F).

407 To minimize neutrophil activation by the presence of serum in the TCM and to mimic the lack of
408 nutrient availability as encountered by cancer cells in an *in vivo* tumor mass, we harvested TCM from
409 cells cultured in 0% serum for 48 hrs (Fig. 2A) – conditions that lead to minimal cell death (Fig. 2B).
410 We found that serum free TCM derived from M4 and MDA-MB-231 cells induced strong neutrophil
411 migration in transwell assays compared to the TCM harvested from MCF-7 cells cultured under the
412 same conditions (Fig. 2C). Notably, a greater percentage of neutrophils migrated toward serum free
413 TCM (Fig. 2C) than to serum reduced TCM (Fig. 1F) derived from either M4 (57% vs. 49%) or MDA-
414 MB-231 (42% vs. 26%) cells. Importantly, a gradual decrease in neutrophil recruitment with serially
415 diluted serum free TCM showed that TCM triggers a dose-dependent response (Fig. 2D). Together,
416 these findings establish that TCM derived from breast cancer cells with triple negative receptor
417 expression status and aggressive malignant potential induce neutrophil polarization and robust
418 migration by secreting specific chemotactic factors. For subsequent studies, we used TCM generated
419 under serum starved conditions from all cell lines.

420 **Neutrophils directionally migrate towards secreted factors harvested from TNBC cell line**

421 We next assessed the ability of TCM to induce neutrophil migration in a more physiologically relevant
422 interstitial tissue-like microenvironment by monitoring neutrophil motility through 3D matrices of
423 type I collagen and time-lapse imaging (Fig. 3A). By tracking the movement of neutrophils, we
424 generated trace plots (Fig. 3B) and rose plots (Fig. 3C) that depict the behavior of cells in response to
425 M4 TCM or media control. CXCL8 was used as a positive control. We found that neutrophils migrated
426 directionally towards M4 TCM compared to media control (Fig. 3Biii, 3Biv, 3Ciii, 3Civ; see also
427 Movie S1&S2). We also found that neutrophils migrated towards M4 TCM with a significantly
428 elevated velocity and directionality, compared to media control (Fig. 3F&3G). These increases in cell
429 velocity and directionality also occurred in response to CXCL8 (Fig. 3Bi, 3Bii, 3Ci, 3Cii, 3D&3E;
430 see also Movie S3&S4). However, a lower directionality was measured in response to M4 TCM (0.1)
431 compared to CXCL8 (0.45), which could reflect the complexity of TCM composition. Indeed, unlike
432 a single chemoattractant like CXCL8, the TCM includes multiple active factors that can potentially
433 modulate their effect and have different diffusibility through the collagen. Taken together, these
434 results indicate that active factors secreted from TNBC cells induce directional migration of
435 neutrophils.

436 **TNBC spheroids secrete factors that recruit neutrophils**

437 We investigated the neutrophil recruitment ability of 3D tumor spheroids generated with breast cancer
438 cell lines. First, we generated tumor spheroids with diameters ranging from 200 to 350 µm using the
439 hanging drop method. Using 2 photon microscopy, we assessed the morphology of the spheroids,
440 which differ in appearance, ranging from irregular, loose aggregates (MDA-MB-231 and BT549) to
441 tight, symmetrical spheres (BT474 and M4) respectively (Fig. 4A, Movie S5-S8). We also determined
442 that under our growth conditions, the spheroids did not harbor a hollow or necrotic core at their center

443 (Fig. 4A), ruling out the possible release of damage-associated molecular patterns (DAMPs) from
444 damaged or dying cells at the spheroid core on neutrophil recruitment [62] (Fig. 4A; Movie S5-S8).

445 To evaluate whether TNBC spheroids secrete neutrophil recruiting factors similarly to TNBC cells
446 grown in monolayers, we assessed neutrophil migration toward spheroid-derived TCM, and found
447 that spheroid-derived TCM from all three TNBC cell lines (M4, MDA-MB-231, and BT549) had
448 neutrophil recruiting activity, while spheroid-derived TCM from the ER+ cell line (BT474) was
449 inactive (Fig. 4B). These results establish that TNBC cells secrete neutrophil-recruiting factors in
450 either 2D or 3D environments.

451 Next, we developed a neutrophil-tumor spheroid co-culture system to monitor the migration of
452 neutrophils towards tumor spheroids by time-lapse imaging (Fig. 5A). During the early hours of
453 imaging, when neutrophils are not activated and therefore not attached to the surface, we noted that
454 the neutrophils followed the fluid flow and some of them non-specifically got trapped on the surface
455 of the tumor spheroids (Movie S9, S10). However, over time, activated neutrophils clearly attached
456 to the surface, actively migrated towards the M4 spheroids, and accumulated around the spheroid
457 boundary (Fig. 5B, Move S9). In contrast, we found that neutrophils never strongly adhered to the
458 surface or directionally migrated towards BT474 spheroids. Instead, they followed the direction of
459 the flow in the system (Fig. 5C, Movie S10). Indeed, quantification of the directionality of neutrophil
460 migration towards the spheroid revealed a higher directionality towards M4 spheroids, compared to
461 BT474 spheroids (Fig. 5D).Taken together, these findings further affirm that TNBC cells induce
462 directional migration of neutrophils by actively secreting specific chemotactic factors.

463 **TNBC cell lines secrete neutrophil activating factors more abundantly than ER+ cancer cell**
464 **lines**

465 One of the major signaling pathways triggered in neutrophils by a wide range of activating factors,
466 including chemoattractants, is the extracellular signal–regulated kinase (ERK) pathway [63, 64]. ERK
467 pathway is also important for activating the migration machinery of neutrophils [65]. We therefore
468 compared the ability of the secreted factors from different breast cancer cells lines to activate ERK
469 by monitoring its phosphorylation status. We found that TCM derived from either M4 or MDA-MB-
470 231 cells induced ERK phosphorylation, with M4 showing a more dramatic response (fMLF and
471 CXCL1 were used as positive controls) (Fig. S3 and 6A). Importantly, we measured no stimulation
472 with TCM derived from the ER+ MCF-7 cells (Fig. S3 and 6A).

473 To identify the nature of the activating factors driving neutrophil migration, we first used multiplex
474 ELISA to quantify the relative presence of potential neutrophil chemoattractants /activators associated
475 with cancer, including a number of CXCL and CCL chemokines, cytokines, and growth factors [1,
476 66] in TCM derived from M4, MDA-MB-231, and ER+ MCF-7 cell lines (Fig. 6B). Among the CXCL
477 chemokines associated with breast cancer of ER- status (GRO, CXCL5, CXCL6, and CXCL8) and
478 breast cancer metastasis (GRO, CXCL5, CXCL6, CXCL8 , and CXCL12) [67, 68], we found a greater
479 than 500-fold increase in GRO chemokines (CXCL1, CXCL2 and/or CXCL3) present in the TCM
480 harvested from TNBC cells, compared to TCM harvested from ER+ cells. This high amount of GRO
481 secretion by TNBC cells is in agreement with the robust expression of CXCL1 mRNA in ER- breast
482 tumor specimen compared to ER+ ones ([55] and Fig. S1). We detected a greater amount of CXCL8
483 present in the TCM from TNBC cells compared to the TCM from ER+ cells, which is in accordance
484 with previous reports [53, 54]. However, compared with GRO chemokines, the fold change in CXCL8
485 expression was more modest, suggesting that CXCL8 is not the key factor involved in neutrophil
486 activation. In addition, we detected very little to no changes for CXCL5 and CXCL6 in any of the

487 TCM. We also measured > 9-fold increase in CXCL12 in the TCM derived from M4 and MDA-MB-
488 231 cells, compared to MCF-7 TCM. In contrast, the CCL family members were in general less
489 abundantly secreted by breast cancer cells. We detected a 5-fold greater abundance of CCL2 in TCM
490 from TNBC cells than ER+ cells, while very little to none CCL3 in any TCM. In contrast, CCL5 was
491 secreted in equivalent amounts by all breast cancer cells, irrespective of the receptor expression status
492 or malignant potential. Other than chemokines, we detected G-CSF and GM-CSF more abundantly in
493 TCM harvested from TNBC cells compared to ER+ cells. Finally, we found that TGF-β1 was 12-30
494 fold more abundant in TCM harvested from TNBC compared to ER+ cells. Taken together, these data
495 show that compared to ER+ breast cancer cells, TNBC cells overexpress a number of potential
496 neutrophil recruiting factors, the most abundant of which being the CXCR2 specific GRO chemokines
497 and TGF-β1.

498 **Tumor derived active factors are of ~12 kDa molecular size**

499 To narrow down our search for tumor-secreted active factors, we used a combination of biochemical
500 and pharmacological approaches. We set out to fractionate the TCM based on the molecular weight
501 of their components and identify the fraction with optimum activity. We subjected the concentrates
502 (>3 kDa) of MDA-MB-231 TCM to size exclusion chromatography (Fig. 7A) and tested the resulting
503 fractions for their ability to induce polarized morphology in neutrophils. We found that the fractions
504 carrying proteins corresponding to ~12 kDa molecular weight (fraction "g" in Fig. 7A) induced
505 maximum polarization as indicated by the elongated shape of the cells (Fig. 7Biv). In contrast, most
506 of the cells retained a circular shape when stimulated with fractions containing proteins that were
507 either larger (Fig. 7Bii&iii) or smaller than ~12 kDa (Fig. 7Bv&vi). Indeed, when we quantified the
508 extent of polarization induced by a series of fractions, we found that circularity was significantly
509 reduced when exposed to MDA-MB-231 TCM itself or TCM-derived fractions corresponding to 12
510 kDa sized proteins (Fig. 7C, fractions e,f,g,h) - A similar pattern of polarized morphology was also
511 induced by M4 TCM derived fractions containing ~ 12 kDa sized proteins (Fig. S5). Importantly, both
512 GRO chemokines [69] and monomeric TGF-β [70] have a molecular weight of 12 kDa.

513 Chemokines activate G protein coupled receptors (GPCR) by signaling through Gi heterotrimeric G
514 proteins, which are sensitive to pertussis toxin (PT) inhibition [71]. To determine the role of
515 chemokines in TCM induced neutrophil migration, we therefore, targeted chemokine specific GPCR
516 Gi signaling by pretreating neutrophils with PT and measured the ability of cells to migrate towards
517 TCM or CXCL8 as a positive control. Using transwell assays, we found that significantly less
518 neutrophils migrated towards TCM derived from either M4 or MDA-MB-231 cells in the presence of
519 PT (Fig. 7D), indicating a role for chemokines in TCM-induced neutrophil recruitment. PT treatment
520 was not toxic, as it did not alter the migration of neutrophils towards the growth factor GM-CSF (Fig.
521 S4). Taken together, these data suggest that chemokines actively contribute to TCM induced
522 neutrophil migration.

523 **The neutrophil recruiting activity of the TCM depends on the combined action of GRO**
524 **chemokines and TGF-β**

525 In order to specifically determine the identity of the mediators, we studied TCM induced neutrophil
526 migration in the presence of different inhibitors targeting either the GRO receptor CXCR2 (AZD 5069
527 [72]) or the TGF-β1 receptor ALK5 (SB431542 [73]), or both. The presence of both inhibitors did not
528 alter neutrophil migration towards fMLF, showing that the inhibitors are receptor specific (Fig. 8A).
529 We found that neutrophil migration induced by M4 TCM remained intact when cells were pretreated

530 with either inhibitor alone (Fig. 8A). In contrast, we noted a significant decrease (~38%) in the
531 percentage of migrating neutrophils towards M4 TCM when cells were pretreated with both inhibitors,
532 indicating that CXCR2 ligands and TGF-β mediate the effects of the TCM (Fig. 8A). Similarly, we
533 found a significant inhibition of M4 TCM induced neutrophil polarization as reflected by the increase
534 in circularity in the presence of both the inhibitors compared to TCM alone (Fig. 8B). However,
535 neutrophil migration induced by MDA-MB-231 derived TCM was not significantly decreased by the
536 inhibitors (Fig. 8A).

537 To further elucidate the role of TGF-β signaling in mediating the effect of TCM on neutrophils, we
538 targeted SMAD3, a downstream signaling component of TGF-β signal transduction pathway [74].
539 Neutrophils pretreated with SIS3 (an inhibitor that specifically inhibits SMAD3 phosphorylation [75])
540 showed intact migration in response to M4 TCM (Fig. 8C). However, when cells were pretreated with
541 inhibitors targeting CXCR2, TGF-β receptor, and SMAD3 phosphorylation, we observed a
542 remarkably stronger inhibition (~60%) of neutrophil migration towards M4 TCM (Fig. 8C) than the
543 inhibition (~38%) measured with CXCR2 and TGF-β receptor inhibitors (Fig. 8A). Importantly, we
544 also found a significant inhibition (~40%) of neutrophil migration towards MDA-MB-231 TCM in
545 the presence of all three inhibitors, compared to vehicle control (Fig. 8D). Together, these results
546 indicate that a concerted action of secreted TGF-β and GRO specific chemokines plays a key role in
547 TCM induced neutrophil recruitment.

548 **Discussion**

549 The purpose of this study was to determine whether neutrophil recruitment in breast tumors is dictated
550 by the malignant potential of breast cancer cells. A number of retrospective studies have reported a
551 unique association of neutrophils with TNBC compared to HR+ subtypes [16, 76, 77]. Using a panel
552 of breast cancer cell lines representing highly aggressive TNBC or poorly aggressive ER+ breast
553 cancer subtypes, we studied tumor driven neutrophil migration in three distinct migration assay
554 systems. We showed a direct causal relationship between the metastatic potential of human breast
555 cancer cells and their ability to recruit neutrophils, and conclude that TNBC subtypes induce robust
556 neutrophil migration by secreting soluble chemical cues. More importantly, we profiled tumor
557 secreted chemical cues with a number of biochemical, pharmacological and immunological
558 approaches and conclude that a unique combination of GRO chemokines and TGF-β are responsible
559 for driving neutrophil recruitment to breast tumor.

560 The primary function of GRO is to guide neutrophil navigate to infection or tissue injury sites. The
561 GRO member CXCL1 has also been implicated to recruit neutrophils in tumor mouse models [52,
562 78]. We measured massive amounts of GRO family chemokines in TCM derived from TNBC cells
563 compared to ER+ breast cancer cells. Yet, surprisingly, we found that TCM activity remains intact
564 after targeting the GRO receptor CXCR2. While GRO chemokines are potent agonists of CXCR2,
565 they can also bind and activate CXCR1, although they have lower affinity towards CXCR1 [79].
566 Furthermore, the rate of ligand induced CXCR1 internalization from the cell surface is relatively
567 slower than that for CXCR2 [80]. Therefore, a potential role of GRO-CXCR1 signaling in mediating
568 the neutrophil recruitment activity of TCM derived from TNBC cell lines cannot be excluded.
569
570 Factors/s other than chemokines may also play a key role to mediate neutrophil migration. In addition
571 to GRO chemokines, we detected considerable amount of TGF-β1 cytokine in the TCM from both
572 M4 and TNBC cell lines. The elevated presence of TGF-β in the tumor niche has been shown to

573 facilitate tumor progression and metastasis in different cancer types [81, 82]. However, TGF-β lacks
574 direct chemoattracting ability for neutrophils [83], which we also verified using recombinant TGF-β
575 in a transwell setup (data not shown). Interestingly, TGF-β was recently shown to promote tumor-
576 permissive phenotypes in TANs [84]. The same study also reported that TGF-β inhibition leads to
577 massive infiltration of cytotoxic neutrophils in tumor-bearing mice. When we inhibited the TGF-β
578 receptor TβRI/type I receptor ALK5, neutrophil migration induced by TCM remained intact.
579 However, targeting both TβRI and CXCR2 led to a significant defect in neutrophil recruitment by M4
580 TCM, but not MDA-MB-231 TCM. Earlier studies identified a novel role of tumor-derived TGF-β in
581 modulating chemokine receptor expression on immune cells [85]. Notably, tumor secreted factors
582 were recently shown to increase expression of TβRI on neutrophils [86]. In line with these previous
583 findings, we envision that TGF-β indirectly promotes TCM induced neutrophil migration through
584 amplification of chemokine signaling. A key mediator in the canonical TGF-β signaling pathway that
585 is critical for TGF-β1-triggered transcriptional regulation is Smad3 [74]. We found that addition of
586 the Smad3 inhibitor disrupted the activity of both M4 and MDA-MB-231 TCM, supporting the notion
587 that TGF-β signaling indirectly promotes neutrophil migration induced by chemokines isolated from
588 TNBC cell lines. We envision that the different amounts of GRO chemokines and TGF-β in M4 and
589 MDA-MB-231 TCM is responsible for the distinct sensitivity between the two TCM. It remains to be
590 determined how TGF-β and chemokine signaling pathways regulate neutrophil migration.

591 While the transwell migration assay is ideal to quantify chemoattracting ability of multiple conditions
592 simultaneously, it lacks the scope to directly monitor migrating cells and assess directionality of cell
593 movement- a true indicator of chemotaxis. The neutrophil recruiting ability of tumor secreted factors
594 collected from lung cancer cell lines has been reported using the underagarose assay [87], which
595 allows to visualize and quantify cell migration [36]. However, we observed no neutrophil migration
596 in response to M4 and MDA-MB-231-derived TCM using the underagarose setup (unpublished). The
597 varying TCM content and diffusability of the secreted factors through the agarose could explain this
598 discrepancy. We did find that the M4 TCM induced neutrophil chemotaxis in 3D collagen matrices
599 that closely mimics interstitial space *in vivo*. By tracking migrating neutrophils, we showed that M4
600 TCM induced neutrophils to migrate with increased velocity and directionality, compared to media
601 control. Using a co-culture system, we also showed that neutrophils migrate directionally toward M4
602 spheroids, while we measured no directional migration toward spheroids in a neutrophil-BT474
603 spheroid co-culture system. Cancer cells grown as 3D spheroids closely mimic the complexity of cell-
604 cell, cell-matrix interactions, and gene expression profiles of the 3D tumor mass *in vivo* [88]. Others
605 have shown neutrophil infiltration into lung tumor spheroids using endpoint imaging of tumor sections
606 [89]. To our knowledge, our study is the first to demonstrate in real time that tumor spheroids actively
607 recruit neutrophils. Whether neutrophils further amplify their chemotactic migration towards tumor
608 spheroids through the secretion of secondary chemoattractants such as leukotriene B_4 or other
609 chemokines in response to tumor-derived factors remains to be addressed [24, 90]. Notably, we found
610 that more neutrophils were present at the 20 hr endpoint in the vicinity of M4 spheroids, compared to
611 BT474 spheroids. Neutrophils have very short life spans, however recent studies point to the role of
612 pro-inflammatory soluble mediators in extending neutrophil survival [64, 91]. Indeed, many of the
613 soluble factors including CXCL8, G-CSF, and GM-CSF, secreted abundantly from the M4 and MDA-
614 MB-231metastatic breast cancer cells, are known to have pro-survival effect on neutrophils [64, 91].
615 Hence, we envisage that the pro-survival effect of M4 secreted factors also underlie the persistence
616 of more neutrophils near M4 spheroids.

617 Much remains to be determined about the mechanisms underlying the secretion of active factors by
618 highly malignant breast cancer cells. Others have shown a critical role of the epithelial-to-
619 mesenchymal transition (EMT) program in promoting tumor metastasis [92, 93]. Through EMT

620 epithelial cancer cells acquire mesenchymal features with enhanced invading properties that aid in
621 cancer cell dissemination. Notably, myeloid cell recruitment was recently detected in EMT marker
622 positive TNBC breast cancer specimen indicating possible role of EMT in tumor-driven neutrophil
623 recruitment [94]. Moreover, EMT associated changes were connected to increased secretion of
624 inflammatory soluble factors including CXCL8 from breast cancer cell lines [94]. Future studies will
625 determine whether turning on EMT also enables breast cancer cells to secrete neutrophil recruiting
626 GRO chemokines and TGF-β. Recently, the release of tumor-derived extracellular vesicles (EVs)
627 have been suggested as a mechanism for the secretion of diverse soluble factors including chemokines
628 and TGF-β [95, 96]. Whether similar mechanisms underlie the secretion of active factors by highly
629 malignant breast cancer cells is the topic of future studies.

630 In conclusion, findings of this study complement previously established role of CXCL chemokines in
631 mediating neutrophil recruitment to tumors, and expand our current understanding by directly linking
632 malignant potential of breast cancer cells with their neutrophil recruiting ability. It is also the first
633 study to unveil a novel role of tumor-derived TGF-β to cooperate with GRO chemokines and
634 orchestrate neutrophil recruitment to TNBC tumors. Future studies will aim to understand how TCM
635 impact the previously described pro-metastasis phenotypes of neutrophils [3, 9-14, 17, 97].
636 Knowledge from this study may help develop novel therapeutic strategies to target neutrophil
637 recruitment to tumors and TAN function, which would restrict metastatic spread without perturbing
638 protective functions of neutrophils against infection and injury.

639 **Abbreviations**

640 **TNBC:** Triple negative breast cancer

641 **ER:** Estrogen receptor

642 **HR:** Hormone receptor

643 **TAN:** Tumor associated neutrophil

644 **TCM:** Tumor conditioned media

645 **f-MLF:** Formyl-methionyl-leucyl-phenylalanine

646 **TGF-β:** Transforming growth factor-β

647 **GRO:** Growth related oncogene

648 **G-CSF:** Granulocyte colony stimulating factor

649 **GM-CSF:** Granulocyte macrophage colony stimulating factor

650 **EMT:** Epithelial-to-mesenchymal transition

651 **PT:** Pertussis toxin

652 **Acknowledgements**

We thank all the members of the Parent laboratory for their insights and suggestions. We are indebted to Dr. Sofia Merajver and Dr. James Rae for kindly providing cell lines. We thank Wu Zhi for thoughtful discussions and isolating TCM. We also thank Kalina Tsolova, Chiamaka Ukachukwu, and Kristen Loesel for assisting in the transwell, underagarose, and 3D migration assays, respectively. We acknowledge Dr. Michael Holinstat and Amanda Prieur from the Platelet Physiology and Pharmacology Core for providing blood draws for this study and thank Peilin Shen for neutrophil isolation and technical assistance. This work was supported by funding from the University of Michigan School of Medicine. .

Figure legends

Figure 1. TCM derived from TNBC cell lines induce neutrophil migration

A. Flowchart describing how TCM was generated and harvested from cell lines grown under serum reduced conditions.

B. Representative maximum intensity projection confocal images showing fixed neutrophils stimulated with (i), DMSO, (ii) 100 nM fMLF, equal volume of (iii) media, (iv) M1 CM or (v) M4 TCM, and stained for F-actin with phalloidin-TRITC (red) and nuclei with DAPI (blue). Scale bars are 12 µm.

C&D. Graphs depicting the circularity (C) and polarization (D) index of neutrophils stimulated with controls or equal volume of TCM derived from different breast cancer cell lines. Each dot represents corresponding value of a single neutrophil for each condition.

E. Cartoon depicting the neutrophil transwell migration assay.

F. Graph depicting the percentage of neutrophils that migrated into the bottom chamber of the transwells containing equal volume of CM from M1 cells or TCM from different breast cancer cell lines. Red and blue bars represent values of neutrophil migration obtained with TCM harvested from TNBC and ER+ cancer cell lines, respectively.

Data shown are mean ± SEM from N=4 (C, D) or 3-15 (F) independent donors represented by individual dots. Each donor (N) represents an independent experiment. ****$P \leq 0.0001$, ***$P \leq 0.001$, *$P \leq 0.05$ when compared with M1 CM (C, D, F) or #### $P \leq 0.0001$ and ### $P \leq 0.001$ when compared with MDA 231 TGL (one-way ANOVA with Dunnett's multiple comparisons test).

Figure 2. TCM derived from serum deprived TNBC cell lines retain neutrophil recruiting ability

A. Flowchart describing how TCM was generated and harvested from cell lines grown under serum free conditions.

B. Graph depicting spontaneous LDH activity in the supernatant of cancer cell lines grown under serum free conditions measured and normalized with respect to maximum LDH activity. Bars represent mean percentage of max LDH activity ± SEM from 3 independent experiments.

C. Graph depicting the percentage of neutrophils that migrated into the bottom chamber of the transwells containing equal volume of TCM from different breast cancer cell lines cultured in serum free condition. Red and blue bars represent values of neutrophil migration obtained with TCM harvested from TNBC and ER+ cancer cell lines, respectively.

D. Graph depicting the percent of neutrophils migrating into the bottom chamber of the transwells containing serially diluted equal volume of TCM from two different TNBC cell lines.

Results are presented as mean ± SEM from N=3-7 (C) or N=3 (D) independent donors represented by individual dots. Each donor (N) represents an independent experiment. **$P \leq 0.005$, *$P \leq 0.05$ when compared with MCF-7 (one-way ANOVA with Dunnett's multiple comparisons test).

697 **Figure 3. Neutrophils directionally migrate towards secreted factors harvested from TNBC cell**
698 **line**
699 **A**. Cartoon depicting the migration chamber used to assess the chemotaxis of neutrophils in 3D
700 collagen matrix towards TCM.
701 **B&C**. Plots showing individual cell tracks (B) and rose plots showing angle histograms of the
702 migrating cells (C) generated from the combined tracks from N=3 independent donors in response to
703 vehicle control (Bi, Ci), 500 nM CXCL8 (Bii, Cii), media control (Biii, Ciii), and M4 TCM (Biv,
704 Civ). Numbers with left and right arrowhead in B represent number of neutrophils moving away and
705 towards different conditions, respectively.
706 **D,E,F,&G**. Graphs depicting velocity (D, E) and X-FMI (F, G) of neutrophils migrating towards 500
707 nM CXCL8 and vehicle control (D,E) or M4 TCM and media (F,G). Each bar represents mean ± SEM
708 from N=3 independent donors with each dot representing average values from independent positions.
709 **** $P<0.0001$, ***$P\leq0.0005$, **$P\leq0.005$ when compared with corresponding control (paired sample
710 t-test).

711 **Figure 4. TNBC spheroids secrete factors that induce neutrophil migration**

712 **A.** Representative 2-photon images of day-4 spheroids stained with the nuclear dye DRAQ5. Each
713 image is from the field of view located at the midpoint between the top and bottom of the z-stack
714 imaging range.
715 **B.** Graph depicting the percentage of neutrophils that migrated into the bottom chamber of the
716 transwells containing equal volume of TCM derived from M4, MDA-MB-231, BT549, or BT474
717 spheroids. Data shown are mean ± SEM from N=6-7 independent donors represented by individual
718 dots. Each donor (N) represents an independent experiment. *$P\leq0.05$ when compared with BT474
719 TCM (one-way ANOVA with Dunnett's multiple comparisons test).

720 **Figure 5. TNBC spheroids actively recruit neutrophils**

721 **A.** Cartoon depicting the co-culture migration system used to assess the chemotaxis of neutrophils
722 towards tumor spheroids in fibronectin coated glass-bottom plate.
723 **B&C.** Representative images of a neutrophil-spheroid co-culture migration assay at 1, 10, and 20 hrs
724 with M4 spheroid (B) or BT474 spheroid (C) at the center of the field of view. Small, dark cells are
725 neutrophils from the same donor. Representative tracks of neutrophils are on the right.
726 **D.** Graph depicting the X-FMI of neutrophils migrating towards M4 or BT474 spheroids. Each bar
727 represents mean ± SEM from N= 3 (BT474 spheroid) or 4 (M4 spheroid) independent donors with
728 each dot representing the average X-FMI for all neutrophils tracked per spheroid. An average of 45
729 neutrophils were tracked per spheroid. ****$P<0.0001$ when compared with BT474 (unpaired t-test).

730 **Figure 6. TNBC cell lines secrete neutrophil activating factors more abundantly than ER+**
731 **cancer cell lines**
732 **A.** Graph depicting pERK1/ERK2 intensity in neutrophils stimulated with controls (fMLF, CXCL1,
733 media) or equal volume of TCM derived from M4, MDA-MB-231, or MCF-7 cells. The quantified
734 pERK1/2 band intensity was normalized to α-tubulin and is shown as mean ± SEM from N=4
735 individual donors represented by each dot. **** $P<0.0001$, **$P\leq0.01$, *$P\leq0.05$ when compared with
736 corresponding vehicle controls (two-way ANOVA with Sidak multiple comparisons test).
737 **B.** Table showing the amount (pg/ml) of chemokines, growth factors and cytokines secreted by M4,
738 MDA-MB-231 and MCF-7 cells determined by multiplex ELISA assay.

739 **Figure 7. MDA-MB-231-derived active factors are ~12 kDa**
740 **A**. Representative size exclusion chromatography elution profile of TCM from MDA-MB-231 cells.
741 **B**. Representative bright field images of neutrophils exposed to vehicle control DPBS (Bi) or TCM
742 peak fractions (fracn) (Bii-vi) as labeled in (A) and corresponding to different molecular weights.
743 **C**. Graph depicting the circularity of neutrophils stimulated with controls (DMSO, fMLF, DPBS,
744 TCM) or equal volume of TCM fractions with gradually decreasing molecular weight. Data show
745 mean ± SEM from N=3 individual donors with two dots for each donor representing mean circularity
746 of all neutrophils in two randomly selected imaging fields. **** P<0.0001, **P≤0.01, *P≤0.05 when
747 compared with DPBS (one-way ANOVA with Dunnett's multiple comparisons test).
748 **D**. Graph depicting the percentage of neutrophils that migrated into the bottom chamber of the
749 transwells containing equal volume of TCM or 20 nM CXCL8 in the presence or absence of PT. Bars
750 show mean ± SEM from N=4-7 individual donors represented by each dot. **P≤0.01, *P≤0.05 when
751 compared with corresponding PT- values (two-way ANOVA with Sidak multiple comparisons test).

752 **Figure 8. The neutrophil recruiting activity of the TCM depends on the combined action of**
753 **GRO chemokines and TGF-β**

754 **A**. Graph depicting the percentage of neutrophils either untreated or pretreated with 1 μM SB, 1 μM
755 AZD, or a combination of 1 μM of SB and 1 μM AZD that migrated into the bottom chamber of the
756 transwells containing equal volume of M4 TCM, MDA-MB-231 TCM, or 100 nM fMLF. Bars show
757 mean ± SEM from N=5-8 donors with each dot representing individual donor.
758 **B**. Graph depicting the circularity of neutrophils exposed to M4 TCM in the presence or absence of a
759 combination of SB and AZD, or with media control. Bars show mean ± SEM from N=3 donors with
760 3-4 dots for each donor representing mean circularity of all neutrophils from at least 3 randomly
761 selected imaging fields.
762 **C&D**. Graphs depicting the percentage of neutrophils migrated into the bottom chamber of the
763 transwells containing equal volume of M4 TCM (C) or MDA-MB-231 TCM (D) in the presence of
764 3 μM SIS3 alone or a combination of 1 μM each of SB, AZD and 3 μM SIS3, or vehicle control. Bars
765 show mean ± SEM from N=4 (C) or 5 (D) donors. **** P<0.0001 when compared with untreated
766 (A), media control (B) (one-way ANOVA with Dunnett's multiple comparisons test). ** P≤0.01 when
767 compared with vehicle control (C-D) (paired sample t-test).

768 **Table 1. Characteristics and culture conditions of the cell lines used in this study**
769 ER, estrogen receptor; PR, progesteron receptor; HER2; human epidermal growth factor receptor 2.
770 Media conditions: FBS, fetal bovine serum; HS, horse serum.* Media supplemented with 10 μg/ ml
771 insulin (Invitrogen), 10 ng/ml EGF (Peprotech), 0.5 mg/ml hydrocortisone and 100 ng/ml cholera
772 toxin (both from Sigma Aldrich). ** Media supplemented with 5 μg/mL insulin, and 1 μg/mL
773 hydrocortisone (Sigma-Aldrich). MCF10A and MCF10CA1a were obtained from Karmanos
774 Research Institute; MDA 231-TGL, MDA 231-BrM2-831, MDA 231-BoM-1833, MDA 231-LM2-
775 4175 were purchased from Memorial Sloan Kettering Cancer Center; SUM-149 was from Dr. Sofia
776 Merajver, University of Michigan; BT549, Hs578T and BT474 were purchased from ATCC; MCF-
777 7, HCC1428, and T47D were kindly gifted from Dr. James Rae, University of Michigan.

Cell lines	ER	PR	HER2	Malignant potential	Culture Media	Serum

MCF10A (M1)	-	-		Benign	*DMEM F12	5% HS
MCF10CA1a (M4)	-	-		Invasive	DMEM F12	5% HS
MDA-MB-231	-	-		More Aggressive	DMEM	10% FBS
MDA-MB-231 TGL	-	-		More Aggressive	DMEM	10% FBS
MDA-MB-231 BrM2-831	-	-		More Aggressive	DMEM	10% FBS
MDA-MB-231 BoM 1833	-	-		More Aggressive	DMEM	10% FBS
MDA-MB-231 LM2-4175	-	-		More Aggressive	DMEM	10% FBS
SUM149	-	-		More Aggressive	**Ham's F12	5% FBS
BT549	-	-		More Aggressive	RPMI	10% FBS
Hs578T	-	-		More Aggressive	DMEM	10% FBS
MCF-7	-	-		Less Aggressive	DMEM	5% FBS
BT474	+	+	+	Less Aggressive	RPMI	10% FBS
HCC1428	+	+		Less Aggressive	RPMI	10% FBS
T47D	+	+		Less Aggressive	RPMI	10% FBS

References

1. SenGupta, S., B.C. Subramanian, and C.A. Parent, *Getting TANned: How the tumor microenvironment drives neutrophil recruitment.* J Leukoc Biol, 2019. **105**(3): p. 449-462.
2. Liew, P.X. and P. Kubes, *The Neutrophil's Role During Health and Disease.* Physiol Rev, 2019. **99**(2): p. 1223-1248.
3. Wculek, S.K. and I. Malanchi, *Neutrophils support lung colonization of metastasis-initiating breast cancer cells.* Nature, 2015. **528**(7582): p. 413-7.
4. Park, J., et al., *Cancer cells induce metastasis-supporting neutrophil extracellular DNA traps.* Sci Transl Med, 2016. **8**(361): p. 361ra138.
5. Zhou, S.L., et al., *Tumor-Associated Neutrophils Recruit Macrophages and T-Regulatory Cells to Promote Progression of Hepatocellular Carcinoma and Resistance to Sorafenib.* Gastroenterology, 2016. **150**(7): p. 1646-1658.e17.
6. Singhal, S., et al., *Origin and Role of a Subset of Tumor-Associated Neutrophils with Antigen-Presenting Cell Features in Early-Stage Human Lung Cancer.* Cancer Cell, 2016. **30**(1): p. 120-135.
7. Berry, R.S., et al., *High levels of tumor-associated neutrophils are associated with improved overall survival in patients with stage II colorectal cancer.* PLoS One, 2017. **12**(12): p. e0188799.
8. Granot, Z., et al., *Tumor entrained neutrophils inhibit seeding in the premetastatic lung.* Cancer Cell, 2011. **20**(3): p. 300-14.
9. Coffelt, S.B., et al., *IL-17-producing γδ T cells and neutrophils conspire to promote breast cancer metastasis.* Nature, 2015. **522**(7556): p. 345-348.
10. Liang, W., Q. Li, and N. Ferrara, *Metastatic growth instructed by neutrophil-derived transferrin.* Proc Natl Acad Sci U S A, 2018. **115**(43): p. 11060-11065.
11. Sasaki, S., et al., *Involvement of Prokineticin 2-expressing Neutrophil Infiltration in 5-Fluorouracil-induced Aggravation of Breast Cancer Metastasis to Lung.* Mol Cancer Ther, 2018. **17**(7): p. 1515-1525.
12. Donati, K., et al., *Neutrophil-Derived Interleukin 16 in Premetastatic Lungs Promotes Breast Tumor Cell Seeding.* Cancer Growth Metastasis, 2017. **10**: p. 1179064417738513.
13. Queen, M.M., et al., *Breast cancer cells stimulate neutrophils to produce oncostatin M: potential implications for tumor progression.* Cancer Res, 2005. **65**(19): p. 8896-904.
14. Kowanetz, M., et al., *Granulocyte-colony stimulating factor promotes lung metastasis through mobilization of Ly6G+Ly6C+ granulocytes.* Proc Natl Acad Sci U S A, 2010. **107**(50): p. 21248-55.

809 15. Shen, M., et al., *Tumor-associated neutrophils as a new prognostic factor in cancer: a systematic*
810 *review and meta-analysis.* PLoS One, 2014. **9**(6): p. e98259.
811 16. Soto-Perez-de-Celis, E., et al., *Tumor-Associated Neutrophils in Breast Cancer Subtypes.* Asian Pac J
812 Cancer Prev, 2017. **18**(10): p. 2689-2693.
813 17. Wang, Y., et al., *Tumor-Contacted Neutrophils Promote Metastasis by a CD90-TIMP-1 Juxtacrine-*
814 *Paracrine Loop.* Clin Cancer Res, 2019. **25**(6): p. 1957-1969.
815 18. Fragomeni, S.M., A. Sciallis, and J.S. Jeruss, *Molecular Subtypes and Local-Regional Control of Breast*
816 *Cancer.* Surg Oncol Clin N Am, 2018. **27**(1): p. 95-120.
817 19. Nasrazadani, A., et al., *Precision Medicine in Hormone Receptor-Positive Breast Cancer.* Frontiers in
818 oncology, 2018. **8**: p. 144-144.
819 20. Yin, L., et al., *Triple-negative breast cancer molecular subtyping and treatment progress.* Breast
820 Cancer Res, 2020. **22**(1): p. 61.
821 21. Schmid, P., et al., *Atezolizumab and Nab-Paclitaxel in Advanced Triple-Negative Breast Cancer.* N Engl
822 J Med, 2018. **379**(22): p. 2108-2121.
823 22. Shaul, M.E. and Z.G. Fridlender, *Neutrophils as active regulators of the immune system in the tumor*
824 *microenvironment.* J Leukoc Biol, 2017. **102**(2): p. 343-349.
825 23. Yang, Q., et al., *The role of tumor-associated macrophages (TAMs) in tumor progression and relevant*
826 *advance in targeted therapy.* Acta Pharmaceutica Sinica B, 2020.
827 24. Subramanian, B.C., R. Majumdar, and C.A. Parent, *The role of the LTB(4)-BLT1 axis in chemotactic*
828 *gradient sensing and directed leukocyte migration.* Semin Immunol, 2017. **33**: p. 16-29.
829 25. Ali, S. and G. Lazennec, *Chemokines: novel targets for breast cancer metastasis.* Cancer metastasis
830 reviews, 2007. **26**(3-4): p. 401-420.
831 26. Yu, P.F., et al., *TNFα-activated mesenchymal stromal cells promote breast cancer metastasis by*
832 *recruiting CXCR2(+) neutrophils.* Oncogene, 2017. **36**(4): p. 482-490.
833 27. Zhou, S.L., et al., *CXCL5 contributes to tumor metastasis and recurrence of intrahepatic*
834 *cholangiocarcinoma by recruiting infiltrative intratumoral neutrophils.* Carcinogenesis, 2014. **35**(3):
835 p. 597-605.
836 28. Li, Y., et al., *Clinicopathological Characteristics and Breast Cancer–Specific Survival of Patients With*
837 *Single Hormone Receptor–Positive Breast Cancer.* JAMA Network Open, 2020. **3**(1): p. e1918160-
838 e1918160.
839 29. Cui, X., et al., *Biology of Progesterone Receptor Loss in Breast Cancer and Its Implications for Endocrine*
840 *Therapy.* 2005. **23**(30): p. 7721-7735.
841 30. Allen, S.G., et al., *Macrophages Enhance Migration in Inflammatory Breast Cancer Cells via RhoC*
842 *GTPase Signaling.* Sci Rep, 2016. **6**: p. 39190.
843 31. Boyum, A., *Separation of blood leucocytes, granulocytes and lymphocytes.* Tissue Antigens, 1974.
844 **4**(4): p. 269-74.
845 32. Subramanian, B.C., K. Moissoglu, and C.A. Parent, *The LTB(4)-BLT1 axis regulates the polarized*
846 *trafficking of chemoattractant GPCRs during neutrophil chemotaxis.* J Cell Sci, 2018. **131**(18).
847 33. Berens, E.B., et al., *A Cancer Cell Spheroid Assay to Assess Invasion in a 3D Setting.* J Vis Exp,
848 2015(105).
849 34. Zhu, X., et al., *Ultrafast optical clearing method for three-dimensional imaging with cellular resolution.*
850 Proc Natl Acad Sci U S A, 2019. **116**(23): p. 11480-11489.
851 35. Roossien, D.H., et al., *Multispectral tracing in densely labeled mouse brain with nTracer.*
852 Bioinformatics, 2019. **35**(18): p. 3544-3546.
853 36. Saunders, C.A., et al., *Genetic manipulation of PLB-985 cells and quantification of chemotaxis using*
854 *the underagarose assay.* Methods Cell Biol, 2019. **149**: p. 31-56.
855 37. Sixt, M. and T. Lämmermann, *In vitro analysis of chemotactic leukocyte migration in 3D environments.*
856 Methods Mol Biol, 2011. **769**: p. 149-65.
857 38. Zengel, P., et al., *μ-Slide Chemotaxis: a new chamber for long-term chemotaxis studies.* BMC cell
858 biology, 2011. **12**: p. 21-21.

859 39. Niggli, V., *Microtubule-disruption-induced and chemotactic-peptide-induced migration of human*
860 *neutrophils: implications for differential sets of signalling pathways.* J Cell Sci, 2003. **116**(Pt 5): p. 813-
861 22.
862 40. Farmer, P., et al., *Identification of molecular apocrine breast tumours by microarray analysis.*
863 Oncogene, 2005. **24**(29): p. 4660-71.
864 41. Minn, A.J., et al., *Genes that mediate breast cancer metastasis to lung.* Nature, 2005. **436**(7050): p.
865 518-24.
866 42. Wang, Y., et al., *Gene-expression profiles to predict distant metastasis of lymph-node-negative*
867 *primary breast cancer.* Lancet, 2005. **365**(9460): p. 671-9.
868 43. Ivshina, A.V., et al., *Genetic reclassification of histologic grade delineates new clinical subtypes of*
869 *breast cancer.* Cancer Res, 2006. **66**(21): p. 10292-301.
870 44. Miyake, T., et al., *GSTP1 expression predicts poor pathological complete response to neoadjuvant*
871 *chemotherapy in ER-negative breast cancer.* Cancer Sci, 2012. **103**(5): p. 913-20.
872 45. Schuetz, C.S., et al., *Progression-specific genes identified by expression profiling of matched ductal*
873 *carcinomas in situ and invasive breast tumors, combining laser capture microdissection and*
874 *oligonucleotide microarray analysis.* Cancer Res, 2006. **66**(10): p. 5278-86.
875 46. Kao, K.J., et al., *Correlation of microarray-based breast cancer molecular subtypes and clinical*
876 *outcomes: implications for treatment optimization.* BMC Cancer, 2011. **11**: p. 143.
877 47. Irizarry, R.A., et al., *Exploration, normalization, and summaries of high density oligonucleotide array*
878 *probe level data.* Biostatistics, 2003. **4**(2): p. 249-264.
879 48. Ritchie, M.E., et al., *limma powers differential expression analyses for RNA-sequencing and*
880 *microarray studies.* Nucleic Acids Res, 2015. **43**(7): p. e47.
881 49. Kaunisto, A., et al., *NFAT1 promotes intratumoral neutrophil infiltration by regulating IL8 expression*
882 *in breast cancer.* Mol Oncol, 2015. **9**(6): p. 1140-54.
883 50. Dominguez, C., et al., *Neutralization of IL-8 decreases tumor PMN-MDSCs and reduces*
884 *mesenchymalization of claudin-low triple-negative breast cancer.* JCI Insight, 2017. **2**(21).
885 51. Yu, P.F., et al., *TNFα-activated mesenchymal stromal cells promote breast cancer metastasis by*
886 *recruiting CXCR2+ neutrophils.* Oncogene, 2017. **36**(4): p. 482-490.
887 52. Acharyya, S., et al., *A CXCL1 paracrine network links cancer chemoresistance and metastasis.* Cell,
888 2012. **150**(1): p. 165-78.
889 53. Lin, Y., et al., *Identification of interleukin-8 as estrogen receptor-regulated factor involved in breast*
890 *cancer invasion and angiogenesis by protein arrays.* Int J Cancer, 2004. **109**(4): p. 507-15.
891 54. Freund, A., et al., *IL-8 expression and its possible relationship with estrogen-receptor-negative status*
892 *of breast cancer cells.* Oncogene, 2003. **22**(2): p. 256-265.
893 55. Yang, C., et al., *CXCL1 stimulates migration and invasion in ER-negative breast cancer cells via*
894 *activation of the ERK/MMP2/9 signaling axis.* Int J Oncol, 2019. **55**(3): p. 684-696.
895 56. Dawson, P.J., et al., *MCF10AT: a model for the evolution of cancer from proliferative breast disease.*
896 Am J Pathol, 1996. **148**(1): p. 313-9.
897 57. Santner, S.J., et al., *Malignant MCF10CA1 cell lines derived from premalignant human breast epithelial*
898 *MCF10AT cells.* Breast Cancer Res Treat, 2001. **65**(2): p. 101-10.
899 58. Neve, R.M., et al., *A collection of breast cancer cell lines for the study of functionally distinct cancer*
900 *subtypes.* Cancer Cell, 2006. **10**(6): p. 515-27.
901 59. Weiger, M.C., et al., *Real-time motion analysis reveals cell directionality as an indicator of breast*
902 *cancer progression.* PLoS One, 2013. **8**(3): p. e58859.
903 60. Bos, P.D., et al., *Genes that mediate breast cancer metastasis to the brain.* Nature, 2009. **459**(7249):
904 p. 1005-9.
905 61. Kang, Y., et al., *A multigenic program mediating breast cancer metastasis to bone.* Cancer Cell, 2003.
906 **3**(6): p. 537-49.
907 62. de Oliveira, S., E.E. Rosowski, and A. Huttenlocher, *Neutrophil migration in infection and wound*
908 *repair: going forward in reverse.* Nature reviews. Immunology, 2016. **16**(6): p. 378-391.

63. Afonso, P.V., et al., *LTB4 is a signal-relay molecule during neutrophil chemotaxis.* Dev Cell, 2012. **22**(5): p. 1079-91.
64. SenGupta, S., et al., *Human neutrophils depend on extrinsic factors produced by monocytes for their survival response to TLR4 stimulation.* Innate Immunity, 2019. **25**(8): p. 473-486.
65. Zhang, E.R., et al., *Chemoattractant concentration-dependent tuning of ERK signaling dynamics in migrating neutrophils.* Sci Signal, 2016. **9**(458): p. ra122.
66. Nagarsheth, N., M.S. Wicha, and W. Zou, *Chemokines in the cancer microenvironment and their relevance in cancer immunotherapy.* Nat Rev Immunol, 2017. **17**(9): p. 559-572.
67. Bièche, I., et al., *CXC chemokines located in the 4q21 region are up-regulated in breast cancer.* Endocr Relat Cancer, 2007. **14**(4): p. 1039-52.
68. Kang, H., et al., *Stromal cell derived factor-1: its influence on invasiveness and migration of breast cancer cells in vitro, and its association with prognosis and survival in human breast cancer.* Breast Cancer Res, 2005. **7**(4): p. R402-10.
69. Mukaida, N., *Chemokines*, in *Encyclopedia of Endocrine Diseases*, L. Martini, Editor. 2004, Elsevier: New York. p. 490-494.
70. Kim, Y.V., et al., *New Strategy for High-Level Expression and Purification of Biologically Active Monomeric TGF-β1/C77S in Escherichia coli.* Molecular Biotechnology, 2015. **57**(2): p. 160-171.
71. Mahadeo, D.C., et al., *A chemoattractant-mediated Gi-coupled pathway activates adenylyl cyclase in human neutrophils.* Mol Biol Cell, 2007. **18**(2): p. 512-22.
72. Nicholls, D.J., et al., *Pharmacological characterization of AZD5069, a slowly reversible CXC chemokine receptor 2 antagonist.* J Pharmacol Exp Ther, 2015. **353**(2): p. 340-50.
73. Halder, S.K., R.D. Beauchamp, and P.K. Datta, *A specific inhibitor of TGF-beta receptor kinase, SB-431542, as a potent antitumor agent for human cancers.* Neoplasia (New York, N.Y.), 2005. **7**(5): p. 509-521.
74. Bierie, B. and H.L. Moses, *Tumour microenvironment: TGFbeta: the molecular Jekyll and Hyde of cancer.* Nat Rev Cancer, 2006. **6**(7): p. 506-20.
75. Jinnin, M., H. Ihn, and K. Tamaki, *Characterization of SIS3, a novel specific inhibitor of Smad3, and its effect on transforming growth factor-beta1-induced extracellular matrix expression.* Mol Pharmacol, 2006. **69**(2): p. 597-607.
76. Liu, C., et al., *Usefulness of neutrophil-to-lymphocyte ratio and platelet-to-lymphocyte ratio in hormone-receptor-negative breast cancer.* Onco Targets Ther, 2016. **9**: p. 4653-60.
77. Pistelli, M., et al., *Pre-treatment neutrophil to lymphocyte ratio may be a useful tool in predicting survival in early triple negative breast cancer patients.* BMC Cancer, 2015. **15**: p. 195.
78. Yuan, M., et al., *Tumor-Derived CXCL1 Promotes Lung Cancer Growth via Recruitment of Tumor-Associated Neutrophils.* J Immunol Res, 2016. **2016**: p. 6530410.
79. Ahuja, S.K. and P.M. Murphy, *The CXC chemokines growth-regulated oncogene (GRO) alpha, GRObeta, GROgamma, neutrophil-activating peptide-2, and epithelial cell-derived neutrophil-activating peptide-78 are potent agonists for the type B, but not the type A, human interleukin-8 receptor.* J Biol Chem, 1996. **271**(34): p. 20545-50.
80. Nasser, M.W., et al., *CXCR1 and CXCR2 activation and regulation. Role of aspartate 199 of the second extracellular loop of CXCR2 in CXCL8-mediated rapid receptor internalization.* J Biol Chem, 2007. **282**(9): p. 6906-15.
81. Yeh, H.W., et al., *A New Switch for TGFβ in Cancer.* Cancer Res, 2019. **79**(15): p. 3797-3805.
82. Luo, J., X.-Q. Chen, and P. Li, *The Role of TGF-β and Its Receptors in Gastrointestinal Cancers.* Translational Oncology, 2019. **12**(3): p. 475-484.
83. Parekh, T., et al., *Neutrophil chemotaxis in response to TGF-beta isoforms (TGF-beta 1, TGF-beta 2, TGF-beta 3) is mediated by fibronectin.* J Immunol, 1994. **152**(5): p. 2456-66.
84. Fridlender, Z.G., et al., *Polarization of tumor-associated neutrophil phenotype by TGF-beta: "N1" versus "N2" TAN.* Cancer cell, 2009. **16**(3): p. 183-194.

958 85. Castriconi, R., et al., *Neuroblastoma-derived TGF-β1 modulates the chemokine receptor repertoire of*
959 *human resting NK cells.* J Immunol, 2013. **190**(10): p. 5321-8.
960 86. Costanzo-Garvey, D.L., et al., *Neutrophils are mediators of metastatic prostate cancer progression in*
961 *bone.* Cancer Immunol Immunother, 2020. **69**(6): p. 1113-1130.
962 87. Sun, B., et al., *Neutrophil Suppresses Tumor Cell Proliferation via Fas /Fas Ligand Pathway Mediated*
963 *Cell Cycle Arrested.* Int J Biol Sci, 2018. **14**(14): p. 2103-2113.
964 88. Katt, M.E., et al., *In Vitro Tumor Models: Advantages, Disadvantages, Variables, and Selecting the*
965 *Right Platform.* Frontiers in bioengineering and biotechnology, 2016. **4**: p. 12-12.
966 89. Tazzyman, S., et al., *Inhibition of neutrophil infiltration into A549 lung tumors in vitro and in vivo using*
967 *a CXCR2-specific antagonist is associated with reduced tumor growth.* Int J Cancer, 2011. **129**(4): p.
968 847-58.
969 90. Lämmermann, T., et al., *Neutrophil swarms require LTB4 and integrins at sites of cell death in vivo.*
970 Nature, 2013. **498**(7454): p. 371-375.
971 91. Colotta, F., et al., *Modulation of granulocyte survival and programmed cell death by cytokines and*
972 *bacterial products.* Blood, 1992. **80**(8): p. 2012-20.
973 92. Tsai, J.H. and J. Yang, *Epithelial-mesenchymal plasticity in carcinoma metastasis.* Genes Dev, 2013.
974 **27**(20): p. 2192-206.
975 93. Ye, X., et al., *Upholding a role for EMT in breast cancer metastasis.* Nature, 2017. **547**(7661): p. E1-e3.
976 94. Suarez-Carmona, M., et al., *Soluble factors regulated by epithelial-mesenchymal transition mediate*
977 *tumour angiogenesis and myeloid cell recruitment.* J Pathol, 2015. **236**(4): p. 491-504.
978 95. Chen, T., et al., *Chemokine-containing exosomes are released from heat-stressed tumor cells via lipid*
979 *raft-dependent pathway and act as efficient tumor vaccine.* J Immunol, 2011. **186**(4): p. 2219-28.
980 96. Szajnik, M., et al., *Tumor-derived microvesicles induce, expand and up-regulate biological activities of*
981 *human regulatory T cells (Treg).* PLoS One, 2010. **5**(7): p. e11469.
982 97. Huo, X., et al., *Transcriptomic profiles of tumor-associated neutrophils reveal prominent roles in*
983 *enhancing angiogenesis in liver tumorigenesis in zebrafish.* Sci Rep, 2019. **9**(1): p. 1509.

Figure 1

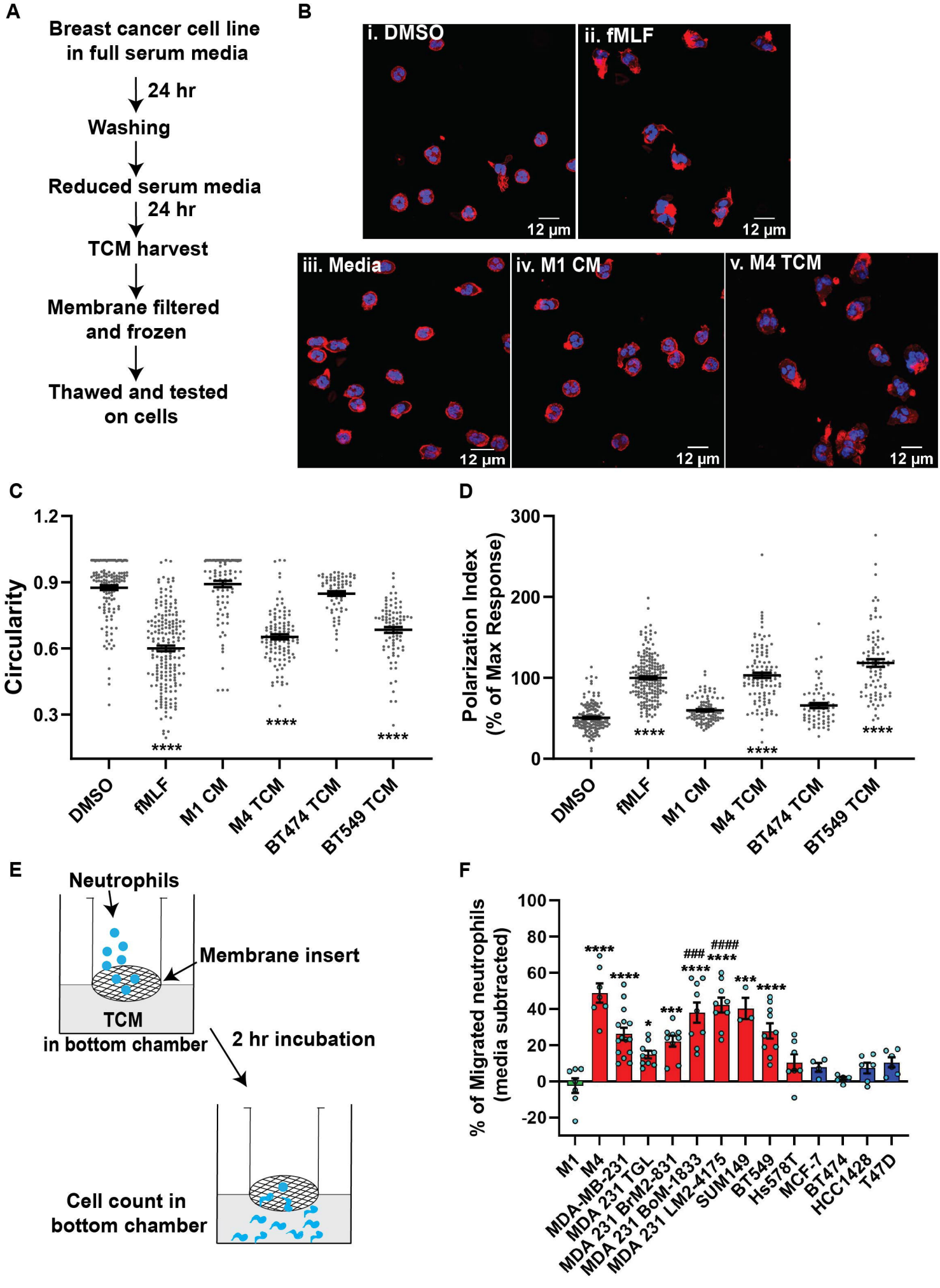
A
Breast cancer cell line in full serum media
24 hr
Washing
Reduced serum media
24 hr
TCM harvest
Membrane filtered and frozen
Thawed and tested on cells
B
i. DMSO
ii. fMLF
iii. Media
iv. M1 CM
v. M4 TCM
12 µm
C
Circularity
DMSO
fMLF
M1 CM
M4 TCM
BT474 TCM
BT549 TCM
D
Polarization Index (% of Max Response)
E
Neutrophils
Membrane insert
TCM in bottom chamber
2 hr incubation
Cell count in bottom chamber
F
% of Migrated neutrophils (media subtracted)
M1
M4
MDA-MB-231
MDA 231 TGL
MDA 231 BrM2-831
MDA 231 BoM-1833
MDA 231 LM2-4175
SUM149
BT549
Hs578T
MCF-7
BT474
HCC1428
T47D

Figure 2

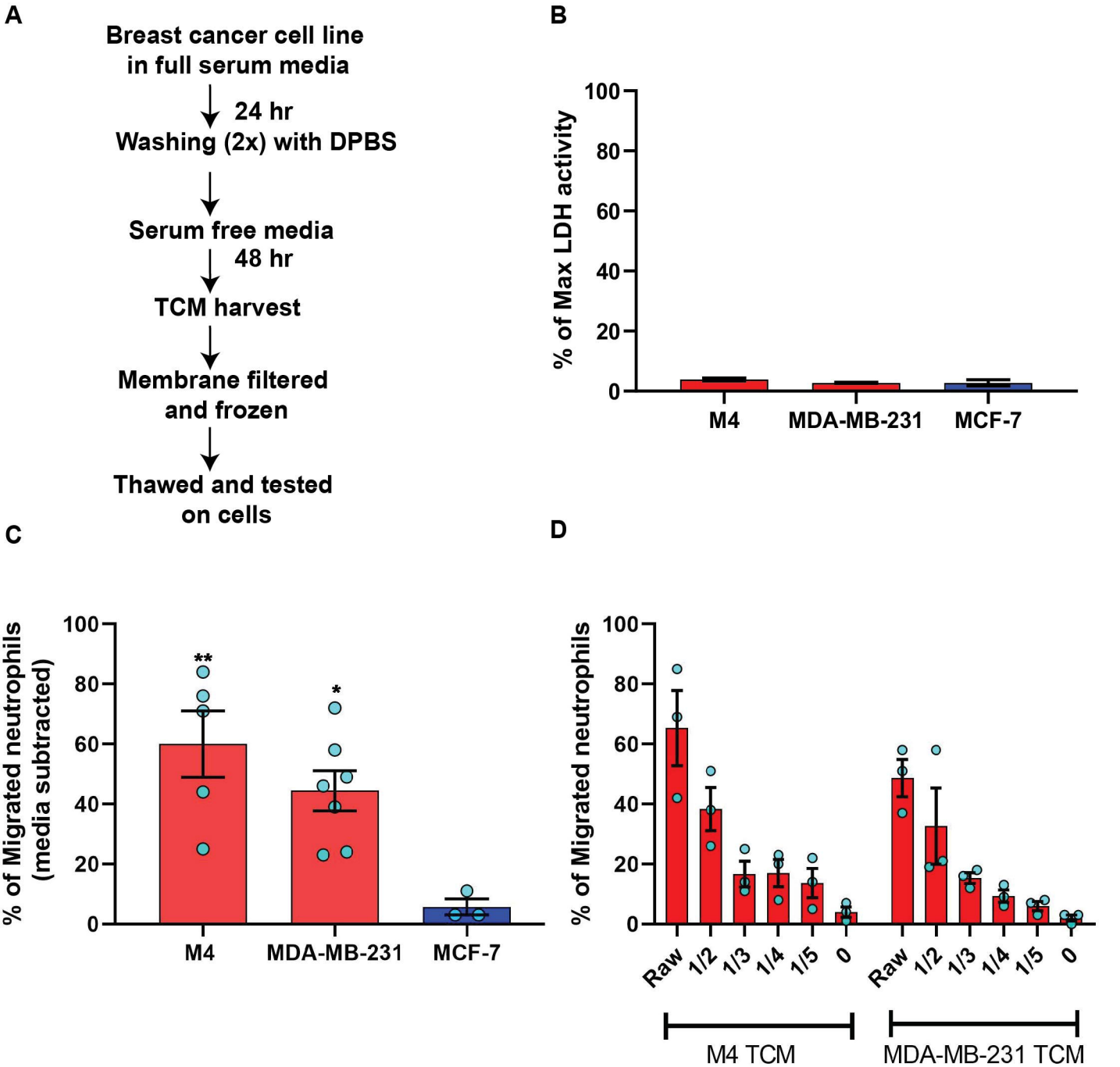
A
Breast cancer cell line
in full serum media
24 hr
Washing (2x) with DPBS
Serum free media
48 hr
TCM harvest
Membrane filtered
and frozen
Thawed and tested
on cells
B
% of Max LDH activity
100
80
60
40
20
0
M4
MDA-MB-231
MCF-7
C
% of Migrated neutrophils
(media subtracted)
100
80
60
40
20
0
**
*
M4
MDA-MB-231
MCF-7
D
% of Migrated neutrophils
100
80
60
40
20
0
Raw
1/2
1/3
1/4
1/5
0
Raw
1/2
1/3
1/4
1/5
0
M4 TCM
MDA-MB-231 TCM

Figure 3

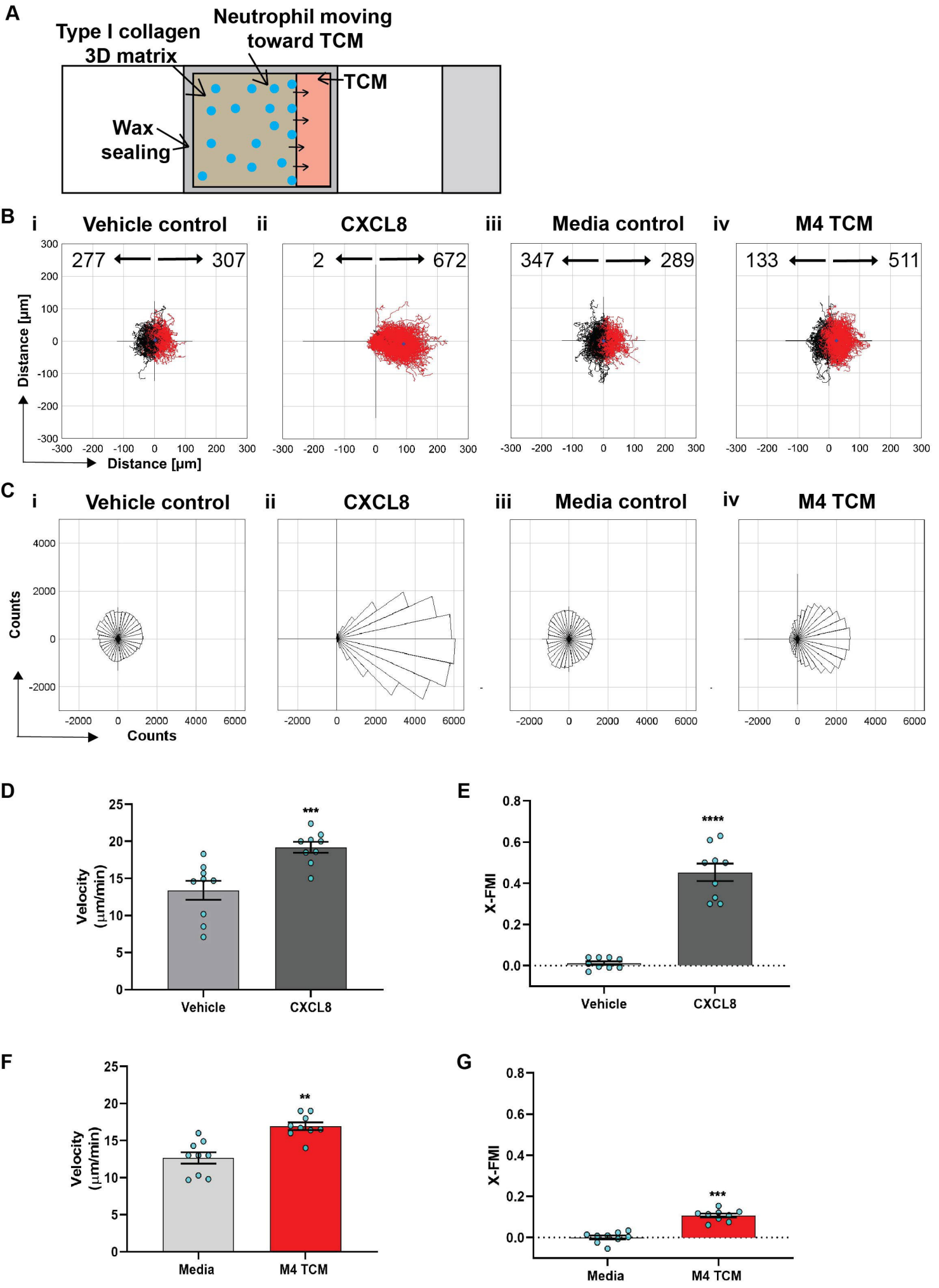
A
Type I collagen 3D matrix
Neutrophil moving toward TCM
TCM
Wax sealing
B
i Vehicle control
ii CXCL8
iii Media control
iv M4 TCM
277
307
2
672
347
289
133
511
Distance [µm]
C
Counts
D
Velocity (µm/min)
Vehicle
CXCL8
E
X-FMI
F
Media
M4 TCM
G

Figure 4

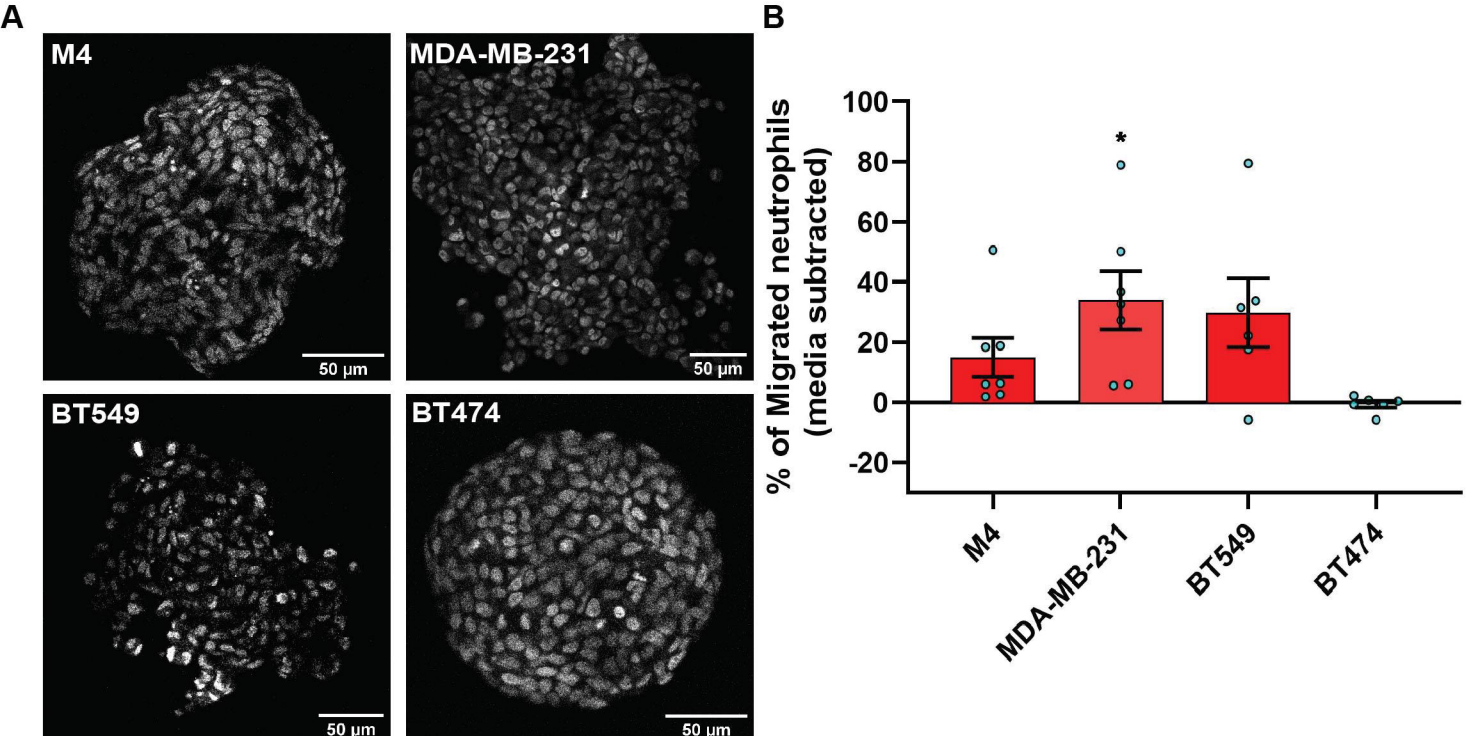
A
M4
MDA-MB-231
BT549
BT474
50 µm
50 µm
50 µm
50 µm
B
% of Migrated neutrophils
(media subtracted)
100
80
60
40
20
0
-20
*
M4
MDA-MB-231
BT549
BT474

Figure 5

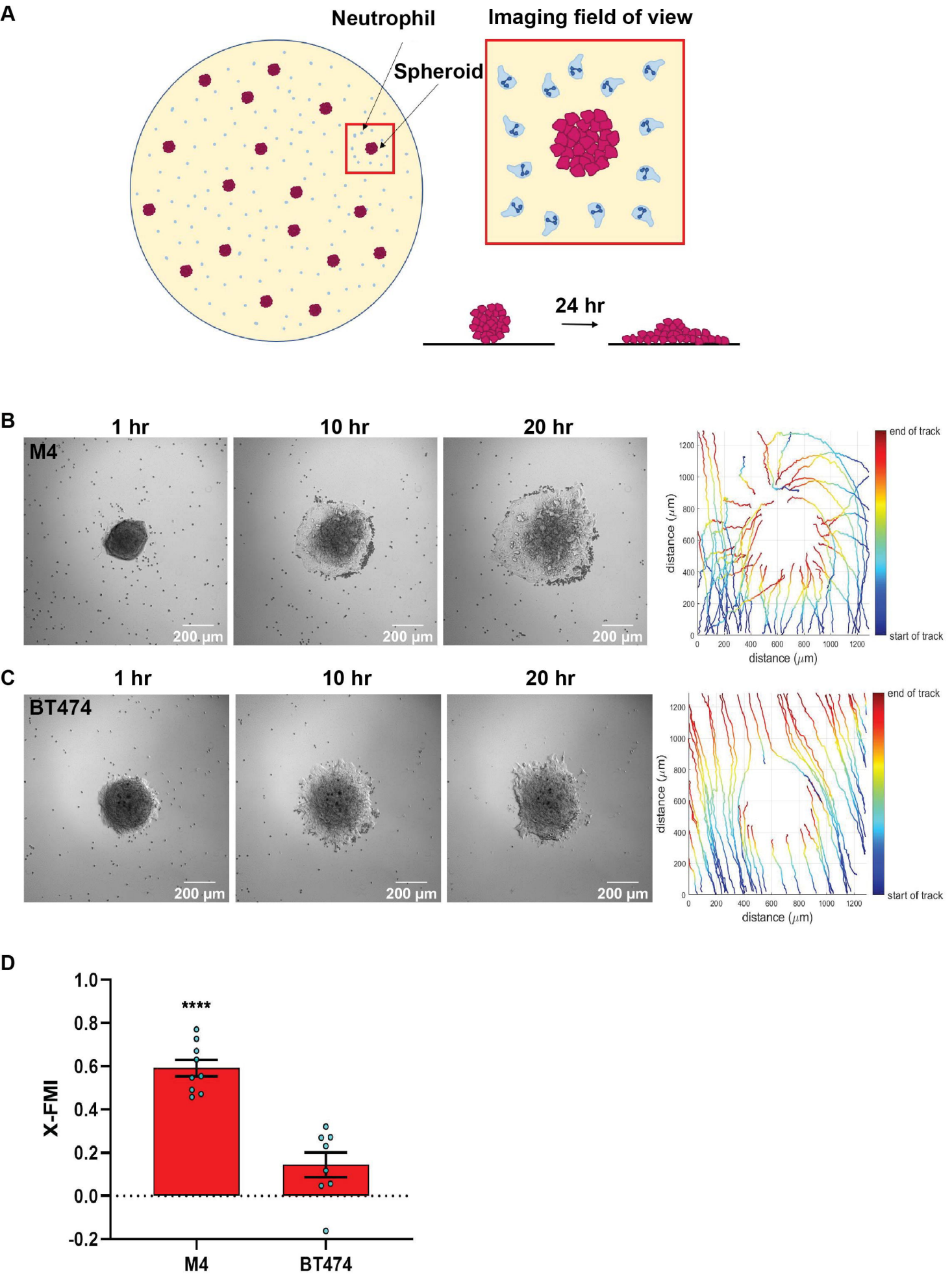
A
Neutrophil
Imaging field of view
Spheroid
24 hr
B
1 hr
10 hr
20 hr
M4
200 µm
end of track
start of track
distance (µm)
C
BT474
D
X-FMI
****
M4
BT474

Figure 6

A

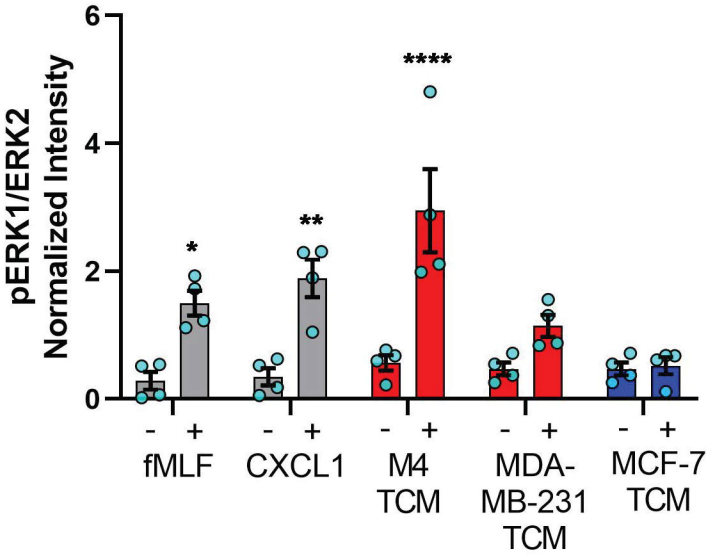

B

Soluble mediators (pg/ml)	M4 TCM	MDA-MB-231 TCM	MCF-7 TCM
GRO (CXCL1/2/3)	>25,000	>25,000	48
CXCL5	5	7	0
CXCL6	0	0	0
CXCL8	>800	455	295
CXCL12	2484	2261	258
CCL2	61	50	11
CCL3	5	11	0
CCL5	252	290	315
G-CSF	294	40	5
GM-CSF	1270	1277	0
TGF-β	>20,000	7998	597

Figure 7

A

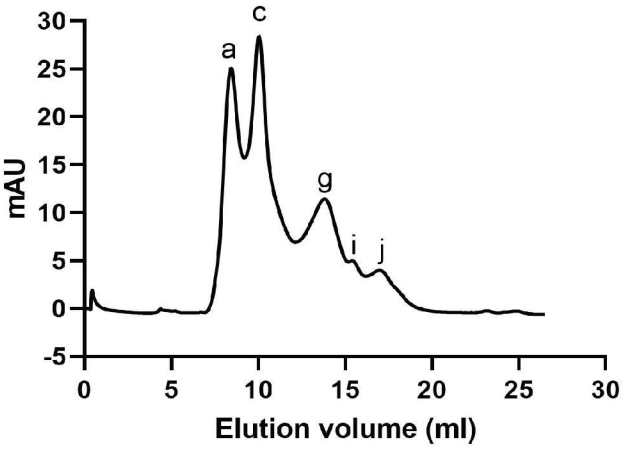

B

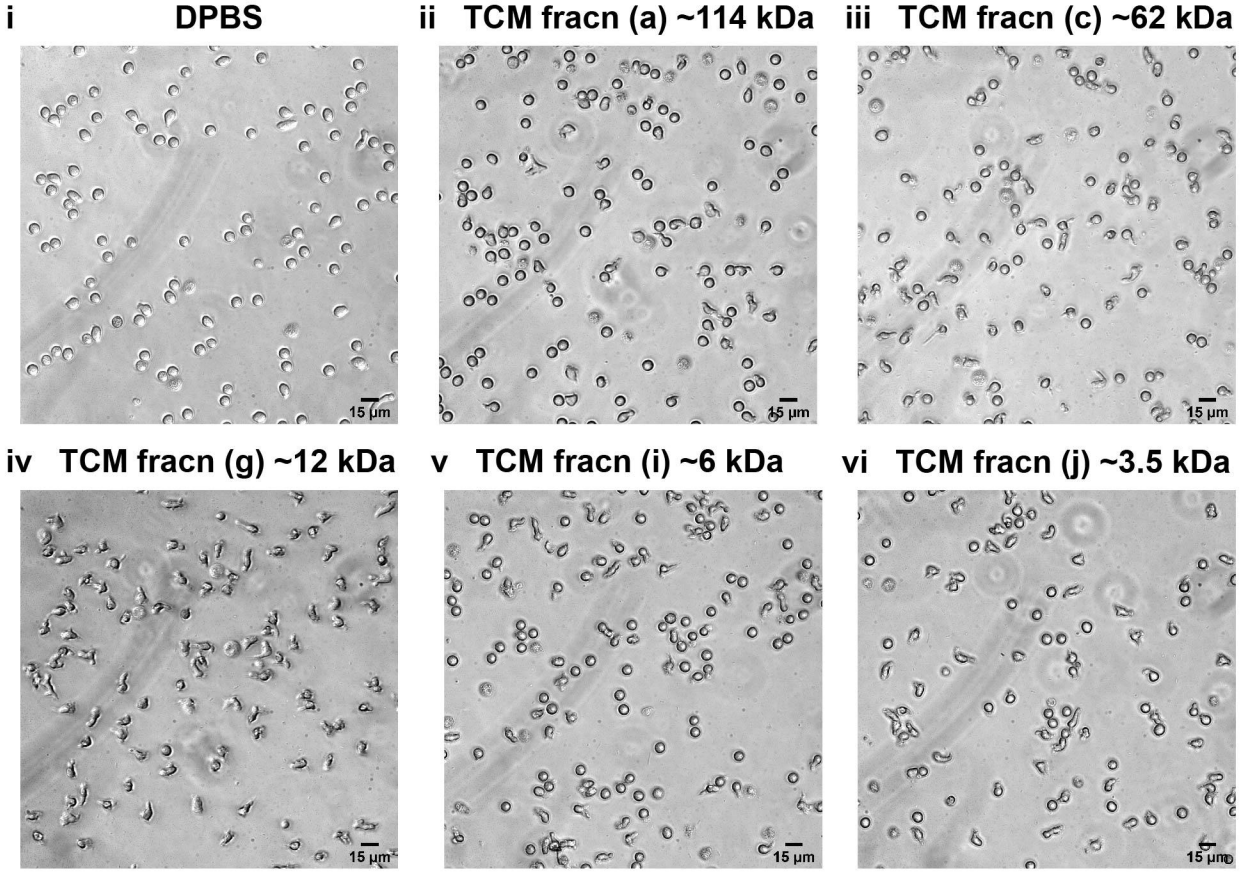

C

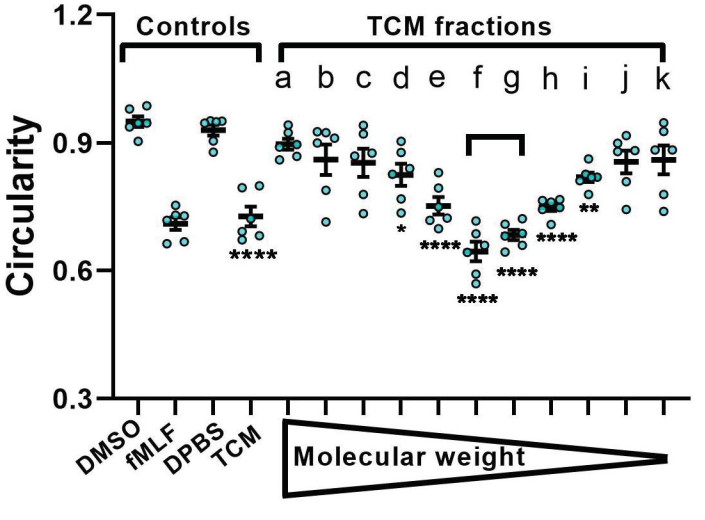

D

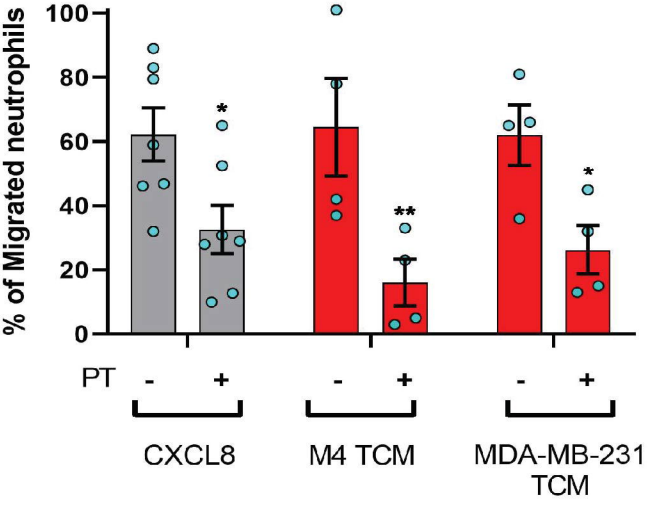

Figure 8

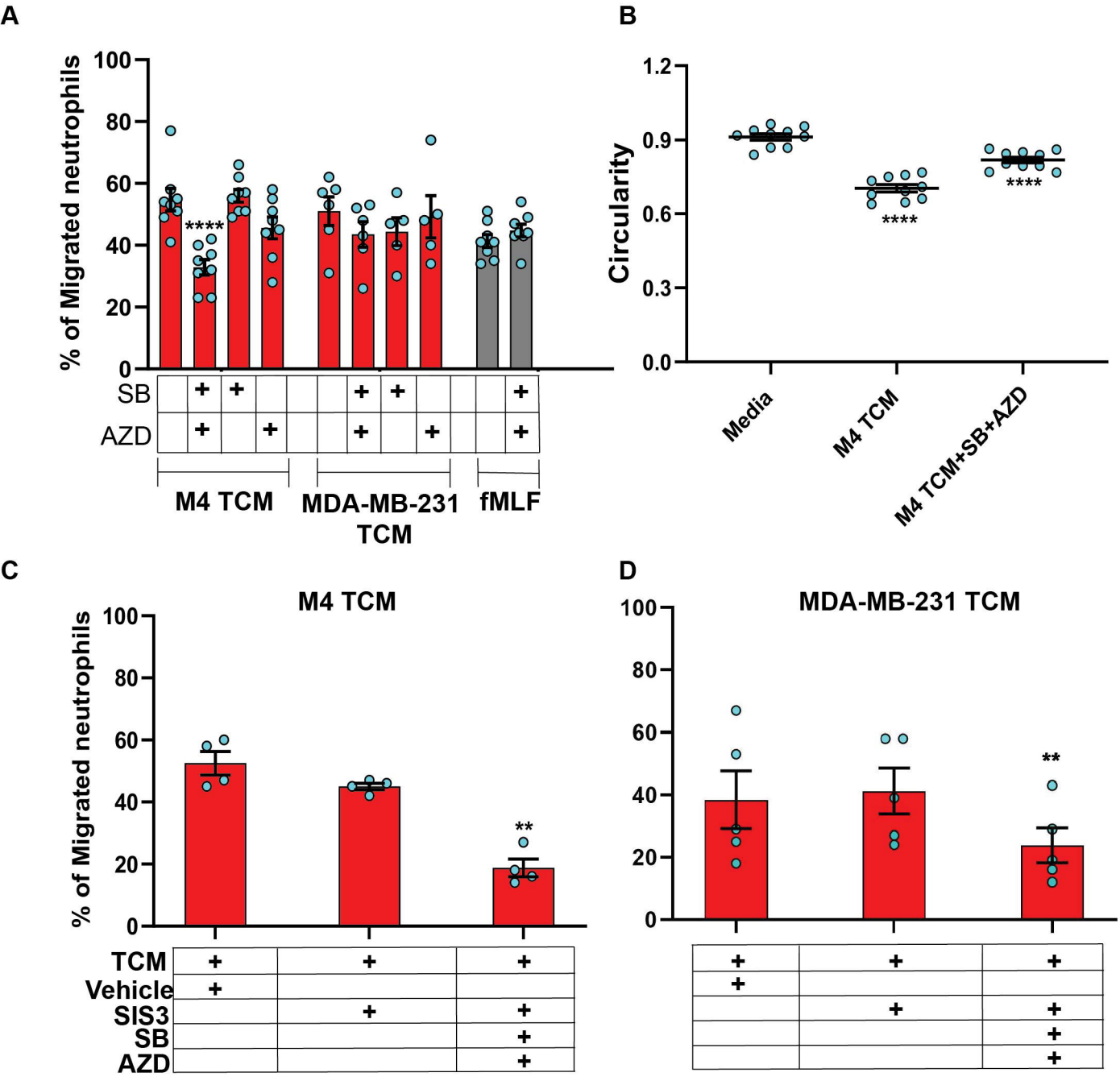
A
% of Migrated neutrophils
100
80
60
40
20
0
****
SB
AZD
M4 TCM
MDA-MB-231 TCM
fMLF
B
Circularity
1.2
0.9
0.6
0.3
0.0
****
****
Media
M4 TCM
M4 TCM+SB+AZD
C
M4 TCM
% of Migrated neutrophils
**
TCM
Vehicle
SIS3
SB
AZD
D
MDA-MB-231 TCM
**